RESEARCH ARTICLE

Key Points:
- Impact ripples, grainfall, and grainflows occur on Martian dunes and are similar to terrestrial counterparts
- Unique, meter-scale large ripples are found on Martian dunes and would distinguish the Martian and terrestrial eolian rock records
- The angle of repose on Martian dunes and large ripples is found to be around 29°, which is similar to that found on Earth

Correspondence to:
R. C. Ewing,
rce@tamu.edu

Sedimentary processes of the Bagnold Dunes: Implications for the eolian rock record of Mars

R. C. Ewing[1], M. G. A. Lapotre[2], K. W. Lewis[3], M. Day[4], N. Stein[2], D. M. Rubin[5], R. Sullivan[6], S. Banham[7], M. P. Lamb[2], N. T. Bridges[8], S. Gupta[7], and W. W. Fischer[2]

[1]Department of Geology and Geophysics, Texas A&M University, College Station, Texas, USA, [2]Division of Geological and Planetary Sciences, California Institute of Technology, Pasadena, California, USA, [3]Department of Earth and Planetary Sciences, Johns Hopkins University, Baltimore, Maryland, USA, [4]Jackson School of Geosciences, Department of Geological Sciences, University of Texas at Austin, Austin, Texas, USA, [5]Department of Earth and Planetary Sciences, University of California, Santa Cruz, California, USA, [6]Department of Astronomy, Cornell University, Ithaca, New York, USA, [7]Department of Earth Science and Engineering, Imperial College London, London, UK, [8]The Johns Hopkins University Applied Physics Laboratory, Laurel, Maryland, USA

Abstract The Mars Science Laboratory rover *Curiosity* visited two active wind-blown sand dunes within Gale crater, Mars, which provided the first ground-based opportunity to compare Martian and terrestrial eolian dune sedimentary processes and study a modern analog for the Martian eolian rock record. Orbital and rover images of these dunes reveal terrestrial-like and uniquely Martian processes. The presence of grainfall, grainflow, and impact ripples resembled terrestrial dunes. Impact ripples were present on all dune slopes and had a size and shape similar to their terrestrial counterpart. Grainfall and grainflow occurred on dune and large-ripple lee slopes. Lee slopes were ~29° where grainflows were present and ~33° where grainfall was present. These slopes are interpreted as the dynamic and static angles of repose, respectively. Grain size measured on an undisturbed impact ripple ranges between 50 μm and 350 μm with an intermediate axis mean size of 113 μm (median: 103 μm). Dissimilar to dune eolian processes on Earth, large, meter-scale ripples were present on all dune slopes. Large ripples had nearly symmetric to strongly asymmetric topographic profiles and heights ranging between 12 cm and 28 cm. The composite observations of the modern sedimentary processes highlight that the Martian eolian rock record is likely different from its terrestrial counterpart because of the large ripples, which are expected to engender a unique scale of cross stratification. More broadly, however, in the Bagnold Dune Field as on Earth, dune-field pattern dynamics and basin-scale boundary conditions will dictate the style and distribution of sedimentary processes.

Plain Language Summary The Mars Science Laboratory rover Curiosity visited two active wind-blown sand dunes within Gale crater, Mars, which provided the first opportunity to make a ground-based observations of sand dunes on Mars. These observations are compared to dunes on Earth and are used as a modern analog for ancient sedimentary rocks on Mars. Dune attributes, such as wind impact ripples and sand flow avalanches, are found to be similar to terrestrial dunes. The avalanches formed between 29 and 40 degrees, which is similar to Earth and supports the idea gravity plays little role in how steeply sand can pile up. The most distinct departure from terrestrial dunes was the presence of meter-scale ripples superimposed on the dunes. This scale of ripple does not exist on terrestrial dunes and is thought to form because of the low-atmospheric density on Mars. This scale of ripple would likely manifest as decimeter-scale wind-blown cross-stratification in the Martian rock record, which is an unusual scale for the terrestrial counterpart.

1. Introduction

Eolian sedimentary environments are now widely recognized across the solar system. Wind-blown bed forms have been identified on the surfaces of Venus, Earth, Mars, Titan, comet 67P/Churyumov-Gerasimenko, and possibly Pluto [*Greeley et al.*, 1992; *Cutts and Smith*, 1973; *Breed and Grow*, 1979; *Lorenz et al.*, 2006; *Mottola et al.*, 2015; *Jia et al.*, 2017; *Moore et al.*, 2017]. Stratification interpreted as eolian in origin has been identified in the rock records of Earth and Mars [e.g., *Brookfield*, 1977; *Grotzinger et al.*, 2005; *Herkenhoff et al.*, 2007; *Grotzinger et al.*, 2015]. The ubiquity of eolian bed forms in the solar system highlights the robust self-organizing nature of the eolian surface sediment transport system within a wide range of planetary boundary conditions [*Kocurek and Ewing*, 2016a].

The Martian surface allows for evaluation of bed forms and stratification developed in low atmospheric density, low gravity, and cold climate boundary conditions owing to the abundant observational and experimental data and subsequently developed theory [*Tsoar et al.*, 1979; *Greeley and Iversen*, 1985; *Grotzinger et al.*, 2005; *Sullivan et al.*, 2008, *Kok et al.*, 2012; *Lapotre et al.*, 2016]. Mars' lower atmospheric density and gravity relative to Earth are fundamental boundary conditions recognized to affect the Martian eolian sediment transport at the grain scale. Higher critical shear stresses are required to lift sand grains at the fluid threshold for transport, and the relatively low critical shear stresses are required to sustain transport at the dynamic threshold [*Greeley et al.*, 1980; *Greeley and Iversen*, 1985, *Kok*, 2010]. These boundary conditions yield clear differences in aspects of the sediment transport system and yield different scales of bed forms from those on Earth [e.g., *Claudin and Andreotti*, 2006; *Sullivan et al.*, 2008; *Pähtz et al.*, 2013; *Durán et al.*, 2014; *Lapotre et al.*, 2016], but surprisingly, although certain attributes of Martian bed form shapes differ, the basic forms remain fundamentally the same.

Studied largely from orbital images and to a lesser extent by lander and rover observations, wind-blown bed forms at the surface of Mars include small and large ripples, coarse-grained ripples, transverse eolian ridges, and dunes [e.g., *Tsoar et al.*, 1979; *Fenton et al.*, 2003; *Balme et al.*, 2008; *Sullivan et al.*, 2008; *Thomson et al.*, 2008; *Ewing et al.*, 2010; *Chojnacki et al.*, 2011; *Bridges et al.*, 2012; *Lapotre et al.*, 2016]. All are recognizable within the range of bed forms found on Earth. Discernable differences in morphology from terrestrial bed forms have been suggested to be due to Martian boundary conditions [*Schatz et al.*, 2006; *Balme et al.*, 2008; *Parteli et al.*, 2014; *Brothers*, 2016], but studies have not demonstrated that morphodynamic feedbacks among the fluid, sand grains, and dune topography associated with self-organizing processes differ enough to generate fundamentally different shaped bed forms. At the field scale, bed form pattern emergence is further spatially and temporally removed from grain-scale processes such that bed form patterns on Mars, characterized by crest line wavelength and defect density, become indistinguishable from those on Earth or any other world [*Ewing et al.*, 2015]. Because the eolian stratigraphic record is thought to form at the pattern scale [*Kocurek and Ewing*, 2016b], the expectation, based on the terrestrial analog, is that eolian stratification on Mars is largely similar to that of Earth's despite differences in boundary conditions.

Stratification interpreted as eolian in origin has been identified in several localities on Mars [*Grotzinger et al.*, 2005; *Herkenhoff et al.*, 2007; *Banham et al.*, 2016; *Bourke and Viles*, 2016]. The Mars Exploration Rover *Opportunity* encountered an outcrop at its landing site within Meridiani Planum which showed an eolian wetting-upward sequence known as the Burns formation [*Grotzinger et al.*, 2005]. The basal stratigraphy consisted of dune-scale cross stratification superposed by parallel-laminated eolian sand sheet-style stratification and capped by sand sheet and interdune stratification [*Grotzinger et al.*, 2005]. The depositional environment was interpreted as a groundwater-influenced wet eolian system. Dune-scale eolian stratification has been recognized within the basal unit of Planum Boreum and within interdunes of the Olympia Undae Dune field in the north polar region of Mars [*Herkenhoff et al.*, 2007; *Ewing et al.*, 2010; *Brothers*, 2016], and satellite imaging and Mars Science Laboratory (MSL) *Curiosity* rover images have revealed eolian stratification in Gale crater, Mars [*Milliken et al.*, 2014; *Grotzinger et al.*, 2015; *Banham et al.*, 2016]. Recently, eolian stratification was identified on the valley floor of Lucaya crater [*Bourke and Viles*, 2016].

That the Martian eolian stratigraphic record is similar to the terrestrial eolian stratigraphic record is the null hypothesis that has guided interpretations of eolian stratification on Mars. However, until now, direct observations of eolian sedimentary processes on dunes were unavailable to test the hypothesis and the extent of applicability of the Earth's analog to Mars' stratigraphic record. Recent observations by Curiosity provide the information needed to answer fundamental questions about Martian bed form development. What scales of bed forms (e.g., ripples and dunes) exist in Martian dune fields that contribute to eolian stratification? Are sedimentary processes on dune lee slopes including grainfall, grainflow, and wind ripples similar in scale and shape to those found on Earth? What controls the distribution of sedimentary processes on a dune and across a dune field?

This manuscript describes and interprets sedimentary processes on two active dunes visited by the Mars rover, Curiosity, in Gale crater, Mars. The work presented here relies chiefly on images returned from orbit and from the suite of cameras on Curiosity. Analysis of the two active dunes illuminates similarities and differences between eolian sedimentary processes on Earth and Mars and allows interpretation of
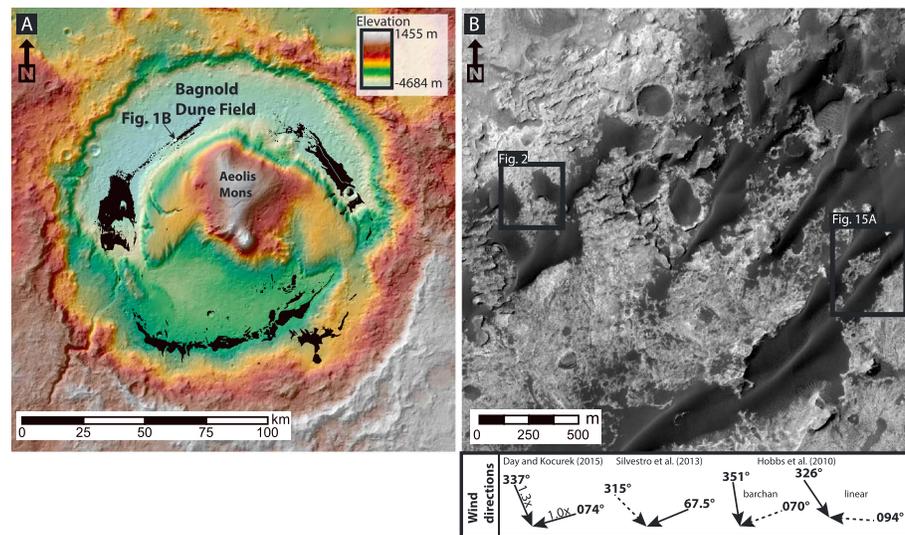
Figure 1. Location map of Gale crater, Mars showing (a) the distribution of dune fields and sand sheets within Gale crater mapped on an High/Super Resolution Stereo Color Imager-generated DEM (modified from *Day and Kocurek* [2015]) and (b) HiRISE satellite image of the study area of Bagnold Dune Field discussed in this work. The study area consists of barchan dunes on the north-northwest flank of the dune field that transition to the southwest into linear dunes. Wind directions over this region as inferred by various authors are shown below Figure 1b. Images: HiRISE ESP_018854_1755.

modern environmental signals of Gale crater from dune and ripple morphologies. This analysis also enables, by analogy with past processes, more informed interpretations of eolian units within the Martian stratigraphic record.

2. The Bagnold Dune Field Study Area

The Bagnold Dune Field sits within Gale crater at the base of the northern flank of Aeolis Mons (i.e., informally Mount Sharp) and is one of several dune fields and sand sheets that surround Mount Sharp (Figure 1a) [*Anderson and Bell*, 2010; *Hobbs et al.*, 2010; *Silvestro et al.*, 2013; *Day and Kocurek*, 2015]. The dune field extends from the NE to the SW and displays barchan and linear dunes as the dominant dune types (Figure 1b). Barchan dunes populate a relatively small fraction of the field at the NNW margin of the dune field and give way to sand sheets and linear dunes to the SSE into the main body of the dune field. The barchan dunes have typical crescentic shapes and strong asymmetric profiles, but, somewhat different from the barchan dune archetype, have two distinct lee slopes that define the downwind sides of the dunes (Figure 2) [*Silvestro et al.*, 2013]. A primary lee slope defines the south-facing crescentic curvature of the dune, and a secondary lee slope flanks their western sides. Linear dunes extend from well-formed sand sheets in the middle of the dune field toward the southwest and are slightly sinuous with two distinct opposing lee slopes oriented toward the northwest and southeast [*Silvestro et al.*, 2013; *Day and Kocurek*, 2015]. In the study area, both barchan and linear dunes are migrating across a bedrock surface and around bedrock buttes, now recognized as the Murray and Stimson formations [*Grotzinger et al.*, 2015].

Curiosity approached the barchan dune margin of the Bagnold dunes from the north as part of a ~ 98 sol campaign (~1162–1260) to investigate the morphology, processes, activity, and composition of an active dune field on Mars (Figure 2) [*Ehlmann and Bridges*, 2017]. The route consisted of a loop between two barchan dunes that exited across its entrance path to continue ascending Mount Sharp. The rover first approached the stoss slope of a barchan dune informally named High Dune before continuing 70 m to the east to the primary lee slope of a barchan dune informally named Namib Dune. From this point, the rover drove to the secondary lee face of Namib Dune to a site informally named Gobabeb for an in situ investigation of the dune and ripple morphology, geochemistry, and grain size [See *Achilles et al.*, 2017; *Elhmann et al.*, 2017; *O'Connell-Cooper et al.*, 2017; *Cousin et al.*, 2017]. Observations of dune slopes, ripples, and interdune areas occurred throughout the campaign using the imaging cameras aboard Curiosity.
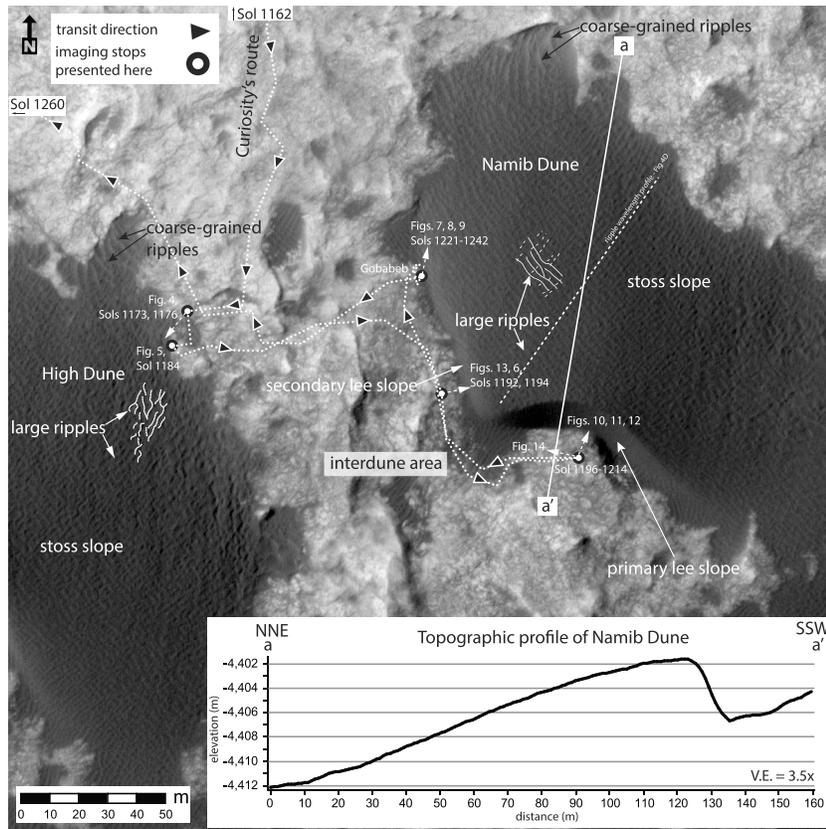
Figure 2. Location map showing the ingress and egress of Curiosity to the field area for the Bagnold Dune campaign (white stippled line; black arrows with white boarder indicate traverse and drive direction). The location of the major stops discussed in this study are noted by white and black circles and labeled by the sols on which the images used in this study were acquired. The location of the figures used throughout the manuscript are labeled along with dune slopes and representative mapping of sedimentary processes visible from HiRISE images. The inset graph shows a profile across Namib Dune to highlight the typical asymmetric dune shape and demonstrate the incline of the underlying bedrock. Images: HiRISE ESP_018854_1755; HiRISE DEM: DTEEC_040770_1755_039280_1755_A01 (1 m/pixel spatial resolution); and HiRISE ESP_039280_1755 was used for dune and ripple measurements collocated with the DEM but is not displayed.

Mesoscale climate models and measurements of bed form morphology, wind speed, wind direction, and sand grain motion indicate that the Bagnold Dune Field is dominated by bimodal winds driven by diurnal forcing within a seasonal wind regime (Figure 2) [*Hobbs et al.*, 2010; *Silvestro et al.*, 2013; *Day and Kocurek*, 2015; *Newman et al.*, 2017; *Bridges et al.*, 2017]. Analyses of slip face dip directions and ripple crest line orientations indicate that the wind modes are from the NW and the ENE with the primary mode from the NW (all wind azimuths in this paper are cited as the direction from which the winds blow) [*Silvestro et al.*, 2013; *Day and Kocurek*, 2015]. A dominant northerly mode is also suggested by mineralogical sorting of olivine to pyroxene across the dune field from the NW toward the SE [*Seelos et al.*, 2014; *Lapotre et al.*, 2017]. Based on mesoscale climate models, the bimodal winds are thought to be driven by diurnal winds moving upslope and downslope over Mount Sharp and the crater rim [*Newman et al.*, 2017]. Based on in situ measurements centered on Ls 90 (southern fall-winter) during Mars Year 33 using the Rover Environmental Monitoring Station (REMS) [*Gómez-Elvira et al.*, 2012], *Newman et al.* [2017] have shown that, in the vicinity of the Bagnold dunes, daily upslope winds blew out on the W and NW and nocturnal downslope winds blew from the E and SE. During the daytime, the wind pattern rotated clockwise giving rise to a morning wind regime dominated by westerly winds and evening winds dominated by easterly winds.

During the same in situ campaign, *Newman et al.* [2017] investigated the wind patterns within the lee side of Namib Dune and found a wider spectrum of winds linked to lee slope turbulence with a dominant westerly mode. The dominance of westerly winds was attributed, in part, to topographic shielding from northerly winds by the dune. Nighttime wind speeds and directions were not fully characterized because of the

rover orientation but indicate some easterly component of the wind. The strength and direction of the diurnal wind patterns may be modulated by seasonal shifts in the regional wind regime, but the winds during the season of Curiosity's visit appeared to be dominated by the diurnal cycle [*Newman et al.*, 2017].

3. Data Sets and Methods

The primary data sets used to assess the sedimentary processes of the Bagnold dunes are High-Resolution Imaging Science Experiment (HiRISE) satellite images, digital elevations models (DEMs) generated from HiRISE stereo pairs, Mast Camera (Mastcam) images, Mars Hand Lens Imager (MAHLI) images, and digital terrain models generated from stereo Mastcam images [*McEwen et al.*, 2007; *Malin et al.*, 2010; *Edgett et al.*, 2012]. HiRISE images are used as a baseline data set for mapping and interpreting differences between ground observations and orbital images. HiRISE DEMs provide topographic data of the dunes.

We used several Mastcam stereo mosaics for high-resolution morphometric analysis. The stereo baseline of the Mastcams is 24.5 cm, while the image targets within these mosaics ranged from 2 to 17 m from the rover. At the outer end of this working distance, errors in determining range from the stereo images are largely in the horizontal direction (unlike an orbital imager, where errors are generally in the vertical direction). This effect causes difficulty in creating an orthoimage that preserves finest-scale ripple morphology. To preserve these details and enable better visual correlation with the original images, we use a smoothing technique prior to image orthorectification. We first rotate the topographic point clouds so that the camera vector aligns with the z axis and then fit a smooth surface to the data using a robust lowess regression model. This smooth surface is then rotated back to the original coordinate system and used for orthorectification of the image data. Our procedure is designed to reduce DEM errors that occur along the direction of the camera vector without unnecessarily distorting the real topography (as would happen if we were to smooth in the original coordinate system). Orthorectified mosaics were gridded at an even spacing of 2–5 mm, consistent with the original image resolution, and at sufficient detail to resolve fine morphologic structures. Rather than conducting analysis directly on this smoothed topographic surface, DEMs are orthorectified via the same procedure to preserve the original small-scale topographic information, at the expense of retaining some high-frequency noise in the data.

All HiRISE and DEM analyses were done using ArcGIS and Qgis. Ripple spacing and grainflow measurements were manually digitized using the orthorectified HiRISE images and orthorectified Mastcam images and DEMS using ArcGIS and MATLAB, with measurements extracted manually by visual inspection using the measure tool.

Grain size distribution was measured using a MAHLI image and a grid-by-number style hand count method [*Bunte and Abt*, 2001]. A regularly spaced grid with a length of twice the diameter of the largest grain in the scene was superimposed on the MAHLI image, and the maximum and intermediate grain diameter of the grain closest to each grid node was recorded for several hundred grains. Grains were assumed to have settled such that the intermediate and maximum axes were orthogonal to the viewing geometry. Uncertainties in the measured particle size result from uncertainties in the MAHLI depth of field used to calculate the image pixel scale.

4. Results

4.1. Stoss Slopes of Namib and High Dunes

The stoss slopes of High Dune and Namib Dune were investigated using HiRISE images and DEMs, and Mastcam images. The size of the dunes and Curiosity's route precluded full imaging of the stoss slopes by the rover cameras, but a lateral and vertical assessment of the slope was made by correlating orbital and ground images. From orbital data, the slope distribution on High and Namib dunes was similar to distributions measured on terrestrial dunes of comparable size and shape (Figures 3a–3c), with stoss slope modes occurring between 7° and 10° [*Finkel*, 1959; *Hesp and Hastings*, 1998]. Topographic profiles showed some variability among the shapes, but within a typical barchan dune range. (Figure 3d) [*Finkel*, 1959; *Hesp and Hastings*, 1998; *Baitis et al.*, 2014].

The most striking aspect of the Namib and High Dune stoss slopes is the superposition of two scales of bed forms on the dune [*Lapotre et al.*, 2016]. Meter-scale bed forms, which are visible from orbit, cover the entire
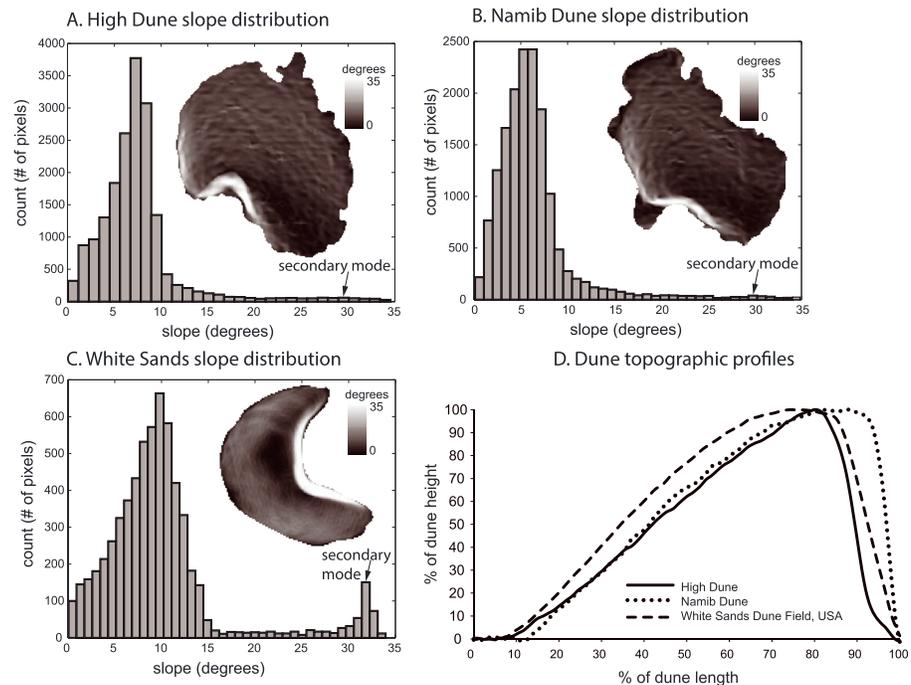
Figure 3. Distribution of slopes on Namib and High Dunes and on a terrestrial barchan dune. Histograms of dune slopes of (a) High Dune, (b) Namib Dune, and (c) White Sands Dune Field, New Mexico, USA show approximately the same stoss slope modes in their distribution. A secondary lee slope mode occurs at the same slope across all histograms, but is somewhat lower and less prominent in the Martian dunes. A black arrow and notation indicating the secondary mode are shown on the histograms. A slope map of the dune cropped from the DEM is subset within each histogram plot. (d) Dune topographic profiles normalized by their length and height for Namib and High Dunes are similar to a representative barchan dune profile from White Sands. Images: HiRISE DEM: DTEEC_040770_1755_039280_1755_A01 (1 m/pixel spatial resolution) (Figures 3a and 3b) and 2010 airborne lidar-derived DEM of White Sands (www.opentopography.org) (Figure 3c).

stoss slope and have been interpreted as large ripples [*Lapotre et al.*, 2016]. Small bed forms, which are only visible from the ground, mantle the large ripples and have been interpreted as impact-generated wind ripples (Figures 4a–4d) [*Lapotre et al.*, 2016]. The term *large ripples* and *impact ripples* are used herein to describe the two different size populations of ripples. In HiRISE images, the large ripples on High Dune and Namib Dune are broadly similar in scale and shape. Large ripples on each dune have a mean wavelength of 2.1 m (*n* = 158) and a distinctive cross-hatch ripple pattern that dominates the dune crest. There, large-ripple crest lines are oriented to the NW and the NE [*Silvestro et al.*, 2013, *Lapotre et al.*, 2016]. Although, the large ripples vary little in wavelength (Figures 4c and 4d), those that occur at the base of the slope have the longest wavelengths and appear slightly brighter overall. These give way to shorter wavelength, darker large ripples within a few meters upslope. Beyond a few meters, no significant variability occurs in large-ripple wavelength upslope (Figure 4d). Variability in large-ripple orientation on High Dune occurs in the transport direction and laterally across the dune. Although a cross-hatch texture is ubiquitous across High Dune, the prominence of the different crest orientations varies. At the dune base, a NE-SW trending crest line pattern is most prominent, which is approximately 40° to the primary slip face dip direction of 190°. Near the crest, a prominent NW-SE trending crest line pattern nearly parallels the slip face.

Mastcam images of the stoss slope of High Dune shows an abrupt transition from the bedrock interdune area to the stoss slope (Figure 4a). The large ripples in this area have sharp crest lines, which are nearly symmetric in profile, a lower angle apron, which defines their basal slopes, and a sand covered interripple area (Figure 4b). The complexity of crest line orientations on High Dune is shown in Figures 4a and 4b where, although a rough trend of crest alignment is apparent, most crest lines intersect other crest lines at angles up to 90°, which gives the ripples a more star-like appearance. At this locality on High Dune, impact ripples form preferentially on the NW flanks of the large ripples, whereas the SE flanks host featureless smooth sand inferred to be grainfall in the leeward side of the large-ripple crests.
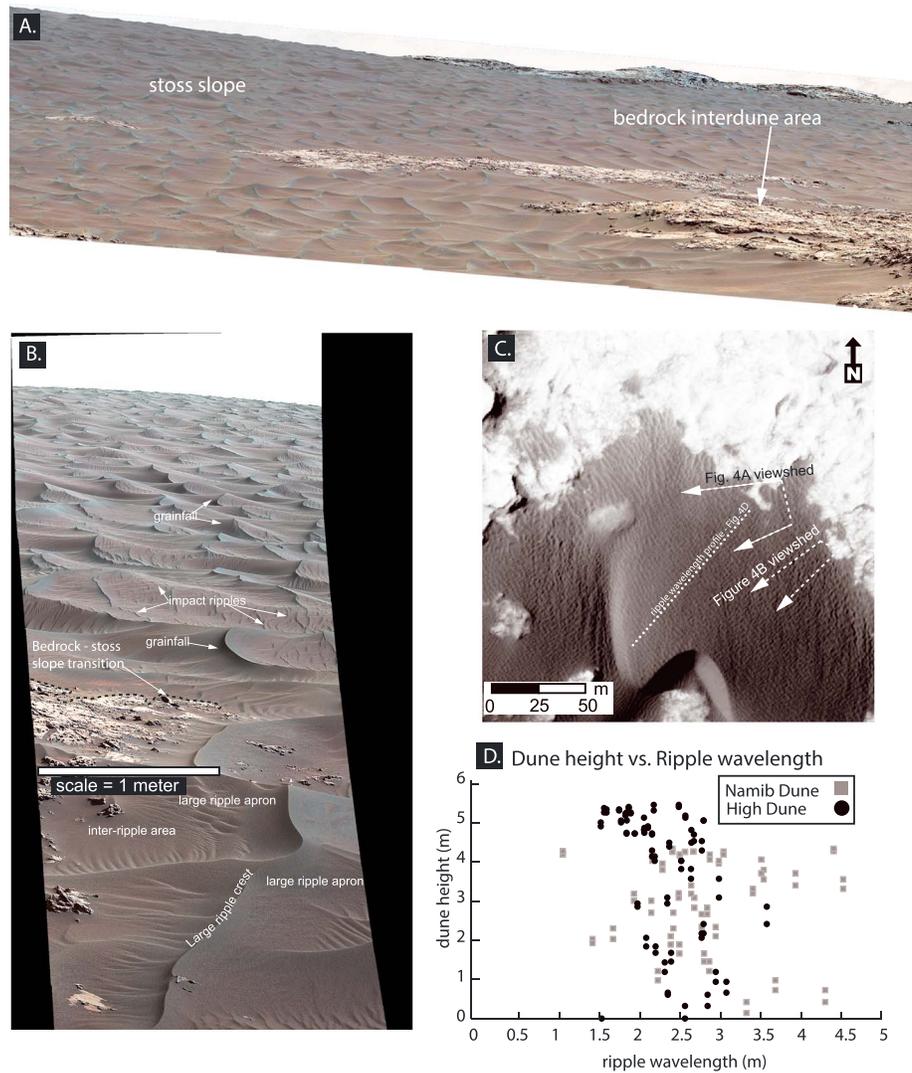
Figure 4. Mastcam and HiRISE images of the stoss slope of High Dune. (a) Mastcam image showing the stoss slope of High Dune and the transition from the bedrock interdune area to the stoss slope. (b) Mastcam image showing ripples at High Dune. Note the sinuous large-ripple crest lines, impact ripples superimposed on the large ripples, and grainfall on the SE side of the large ripples. (c) HiRISE image showing the approximate same area as the Mastcam images. The largest ripples at the base of High Dune are brighter and straighter crested than those higher on the dune. (d) Plot of position of ripple on relative dune elevation versus wavelength along the stoss slope of Namib and High Dunes shows the lack of a trend in wavelength up the slope. This differs from superimposed dunes on Earth, which change wavelength over distance [*Ewing and Kocurek*, 2010]. Images: mcam05312, Sol 1173 (Figure 4a); mcam_05329, Sol 1176 (Figure 4b); HiRISE image: ESP_018854_1755 (Figure 4c); DTEEC_040770_1755_039280_1755_A01 (1 m/pixel spatial resolution) and HiRISE ESP_039280_1755 were used for the collocated dune and ripple measurements but are not displayed.

At Curiosity's closest approach to High Dune, Mastcam stereo and MAHLI high-resolution images characterized detailed ripple morphology and grain size (Figure 5a). Geochemical analysis by the Curiosity Chemical Camera (ChemCam) [*Maurice et al.*, 2012] was also done here on targets named Barby and Kibnas (Sols 1184–1186) and is described by *Cousin et al.* [2017] and *Elhmann et al.* [2017]. The Mastcam images show distinct grain size differences between the large-ripple crest, basal apron, and interripple areas (Figure 5a). Qualitatively, coarser grains are more common at the crest and interripple areas than on the flanks. Total relief on the large ripple is 12 cm (Figure 5b). The large-ripple profile indicates a slight asymmetry toward the east at the crest (Figure 5b). Impact ripples within the interripple area and on the flanks of the large ripple have an average wavelength of ~8 cm [*Lapotre et al.*, 2016].
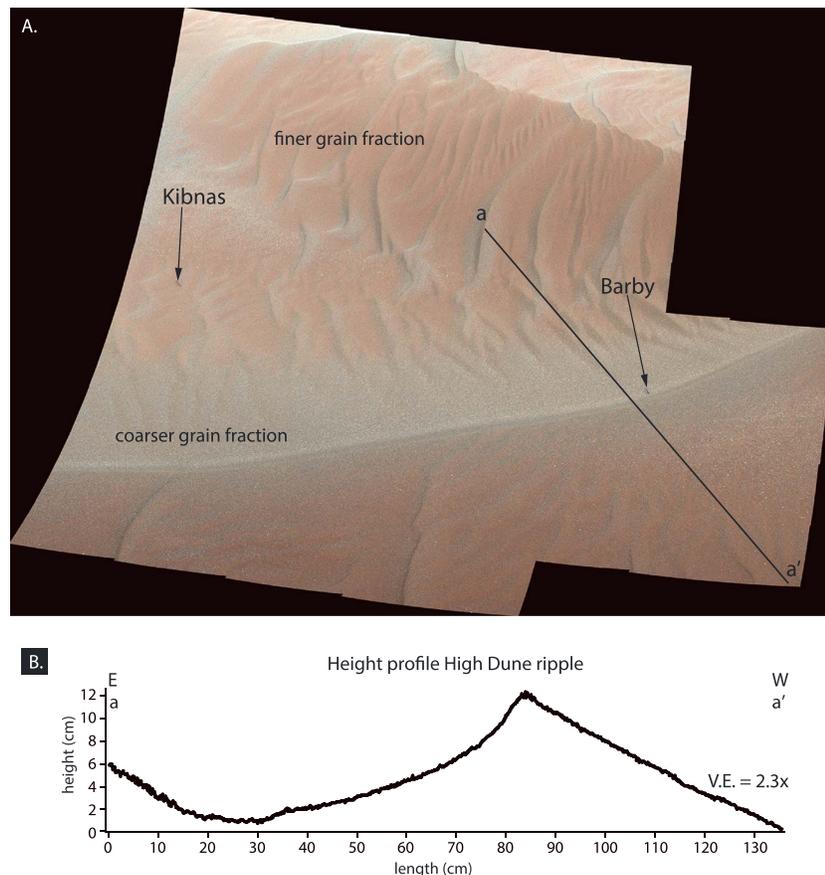
Figure 5. Large ripple at the base of High Dune. (a) Mastcam mosaic of a ripple. Note the coarser-grained crest and interripple area as compared to the finer-grained slope of the ripple. Note the greater abundance of coarser grains on the east facing slope of the ripple. Barby and Kibnas refer to ChemCam targets to assess the chemistry of the sand [*Cousin et al.*, 2017]. (b) Topographic profile of the ripple from a DEM derived from Mastcam stereo images. The east facing side of the ripple crest is slightly oversteepened. The total ripple height is around 12 cm from the trough. Images: mcam05372, Sols 1184 (Figure 5a).

The stoss slope-to-crest area of Namib Dune was imaged from the interdune area between High Dune and Namib Dune as Curiosity navigated toward the lee slope of Namib Dune (Figures 2 and 6). The large ripples atop Namib Dune have sinuous crest lines, but, unlike the ripples at the base of High Dune, are strongly asymmetric in their profile and have distinctive stoss and lee slopes. The large-ripple stoss slopes are mantled by impact ripples that contour over and around the large-ripple crests and lee slopes. The lee slopes exhibit grainflow, grainfall, and impact ripple sedimentary processes. Grainflows on the large-ripple lee slopes occur as translational slides in which part the lee slope surface detaches from the underlying slope and moves downslope as a cohesive block. More typical sand flow avalanches are also present with concave amphitheater-headed scarps at their source and convex-shaped toes that reach to the base of the ripple. Grainfall is indicated in the smooth, featureless areas of the large-ripple slip faces. Mastcam multispectral images show grain color differences within the grainflow and grainfall, which imply some sorting by size and density [*Johnson et al.*, 2017]. Although the large ripples on Namib Dune have a strong asymmetry and are dominated by NW-SE oriented crests, secondary crest lines orthogonal to this orientation are visible in the Mastcam images (Figures 4a and 4b) and likely account for the cross-hatch pattern observed in HiRISE (Figure 2).

Located at the western margin of the secondary slip face of Namib Dune, the Gobabeb site was the final area visited by Curiosity before departing Namib Dune. At this site, Curiosity's scooping campaign evaluated the relationship between mineralogical variations and grain size [see *Achilles et al.*, 2017] and imaged the grain size of the ripples and scoop dump piles [*Elhmann et al.*, 2017; *Edwards et al.*, 2017]. Gobabeb is located near the intersection of the edge of the secondary lee slope, the upper stoss slope, and the dune crest.
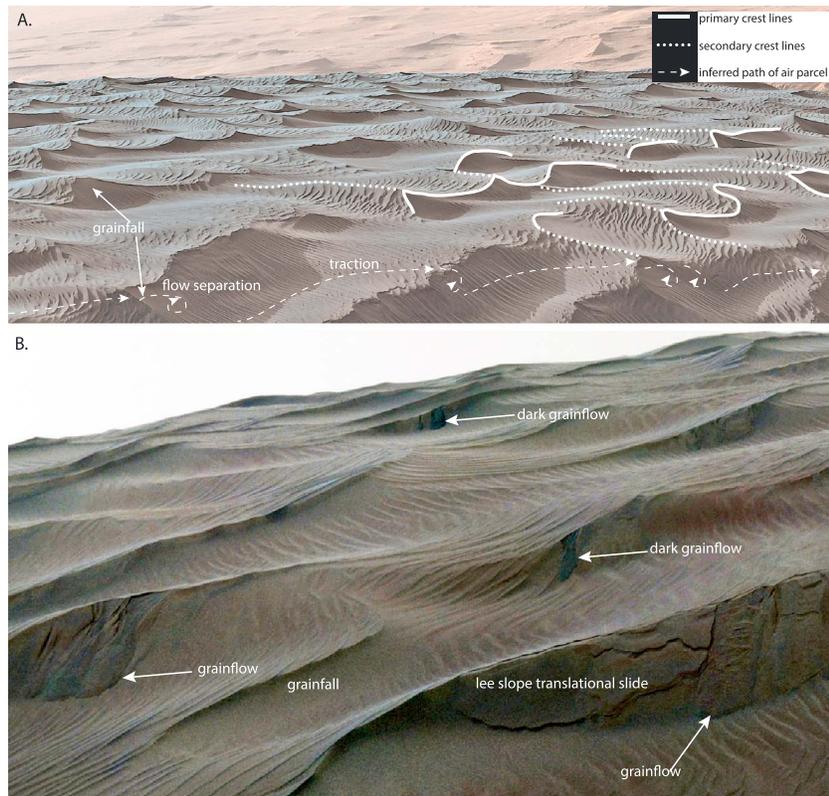
Figure 6. Mastcam image of the crestal area of Namib Dune. (A) Mastcam image highlighting sinuous crest lines and the asymmetry of the ripples. The solid lines trace primary large-ripple crest lines and the stippled lines indicate secondary, crest lines orthogonal to the primary crest lines that likely form the cross-hatch pattern seen in HiRISE images (Figure 2). The dashed white arrows show the airflow pathway over the ripples based on the sedimentary processes visible. Grainfall indicates the presence of flow expansion and lee slope ripples indicate secondary, deflected flow. (b) Mastcam image of the ripples on the stoss slope-to-crest area of Namib Dune. Different styles of grainflows are present typical "hourglass shaped" and translational slides. Differences in the color of the grainflows may indicate the relative activity of the flows, where the darker grainflows are likely younger. Images: mcam05410, Sol 1192 (Figure 6a).

Large ripples and impact ripples were examined in detail at the Gobabeb site (Figure 7). The large ripples in Figure 7a are spaced ~2 m apart and have a clear asymmetry defined by stoss and lee slopes. The stoss slopes are mantled by impact ripples, which contour over and around the large-ripple topography. The impact ripples intersect the largest ripple crest lines obliquely such that the impact ripples are migrating along the large-ripple crest (Figures 7a and 7b). The impact ripples terminate at the brinkline of the large ripple and give way downslope to grainflow and grainfall. Where the rover wheel scuffed the ripple and exposed a cross section of impact ripples, millimeter-scale, parallel laminations are apparent in the upper centimeter and interpreted as stratification developed by the migration of the impact ripples (Figure 7c). The defects or termination of the large ripples are curved to become parallel with the impact ripples and appear to be being reworked by the impact ripples (Figure 7a).

Similar to the large ripples atop the crest of Namib Dune, the Gobabeb large ripples have both grainfall and grainflow on their lee slopes. Grainfall forms the smooth and featureless areas on the lee slope that are punctuated along slope by grainflows with a typical hourglass shape, which extends from large-ripple brink to base. The grainflows show a typical thickened toe region that tapers to a wedge. The flows downlap onto the basal apron where the toes are overprinted by and interfinger with along-slope migrating impact ripples. Some degree of grain sorting by the avalanche process is inferred by color differences between the flow edges and their interiors with the expectation that relatively coarser grains are more abundant in the toes than elsewhere (Figures 7a and 7b) [Allen, 1970]. Where the rover scuffed the large ripple and triggered grainflows, this type of sorting was visible as coarse, white grains, interpreted to be calcium
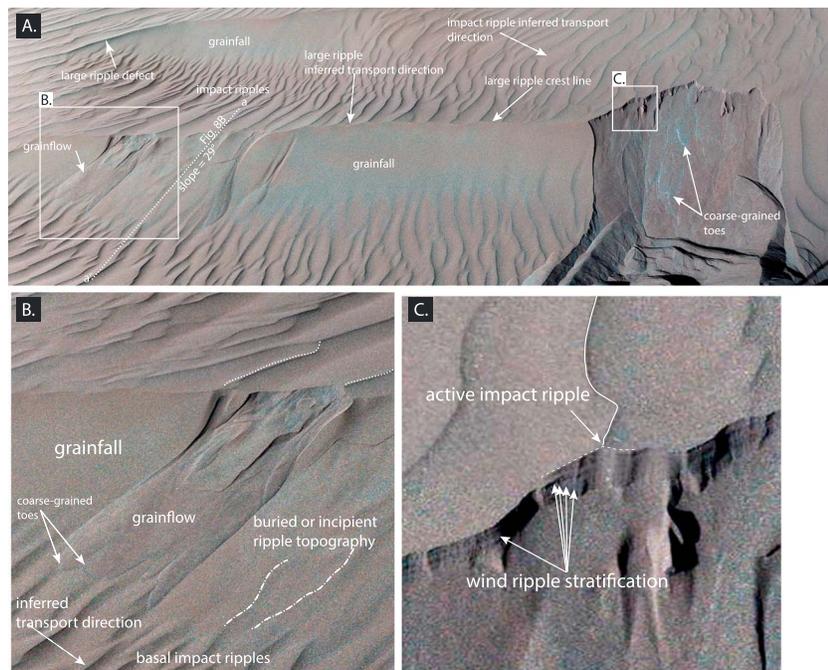
Figure 7. Large ripples and impact ripples at the Gobabeb site on Namib Dune. (a) Two prominent large ripples at Gobabeb show a strong asymmetry and evidence of feedback between ripple topography and airflow where impact ripples are deflected by the large ripple, and grainflow and grainfall form on the lee slope. Note the orientation of the small ripples on the stoss slopes of the ripples are oblique to the primary crest line orientation. (b) A zoomed portion of the same Mastcam image showing the details of the grainflow and interfingering of grainflow and along-slope migrating small ripples. Color differences at the edge of the grainflow shown in Figure 7a may indicate sorting of grains during the avalanche process. (c) Millimeter-scale parallel lamination exposed in a wheel-trench superposed by impact ripples and interpreted to be wind-ripple stratification generated by the migration of impact ripples. Images: mcam05600, Sol 1221 (Figures 7a–7c).

sulfate deflated from the interdune bedrock, preferentially concentrate at the edges of the flows (Figure 7a) [*Bridges et al.*, 2017; *Elhmann et al.*, 2017].

On Sol 1242, an undisturbed ripple crest (target "Otavi") near Gobabeb (Figure 8a) was imaged with MAHLI from a ~ 1 cm standoff distance at a spatial resolution of ~16 ± 0.2 μm per pixel (Figure 8b). The diameter of grains at Otavi ranges from coarse silt to medium sand (e.g., ~50 to 350 μm) (Figure 8c). The average maximum and intermediate axis diameters were measured as fine sand 135.4 ± 1.7 μm and very fine sand 113.6 ± 1.4 μm, respectively. The median intermediate axis was measured as 102 μm. No spatial variation in grain size was observed across the ripple. A similar size distribution from this area was also found by *Sullivan and Kok* [2017].

A DEM generated from Mastcam stereo images was used to extract large-ripple topography at Gobabeb (Figure 9). Figure 9a shows the area prior to the rover scuff and scooping activity. A profile across the large ripple in the background of Figure 9a shows a relatively flat stoss slope, a steep lee slope (Figure 9b), and a maximum relief of 28 cm. The steepest part of the profile reaches 29°, which is consistent with the presence of grainflows on the ripple slope. The large ripples in the foreground are spaced 1.4 m apart and have lower angled lee slopes than the large ripple shown in Figure 9b (Figures 9c and 9d). The relief on the large ripple in Figure 9c ranges up to 16 cm, and the slope profile shows a steep upper slope that reaches ~25° and gives way downdip to a shallower basal apron. The large-ripple profile shown in Figure 9d has a maximum relief of 12 cm and a shallow, consistent overall lee slope at 15° with no apparent steep upper area. Neither large ripple shown in Figures 9c or 9d has grainflows, but, based on the images, both have smooth, featureless sand characteristic of grainfall in their lee.

4.2. Lee Slope of Namib Dune

The primary and secondary lee slopes of Namib Dune were investigated using HiRISE and Mastcam images, as well as DEMs derived from each of these instruments. The primary lee slope of Namib Dune measured
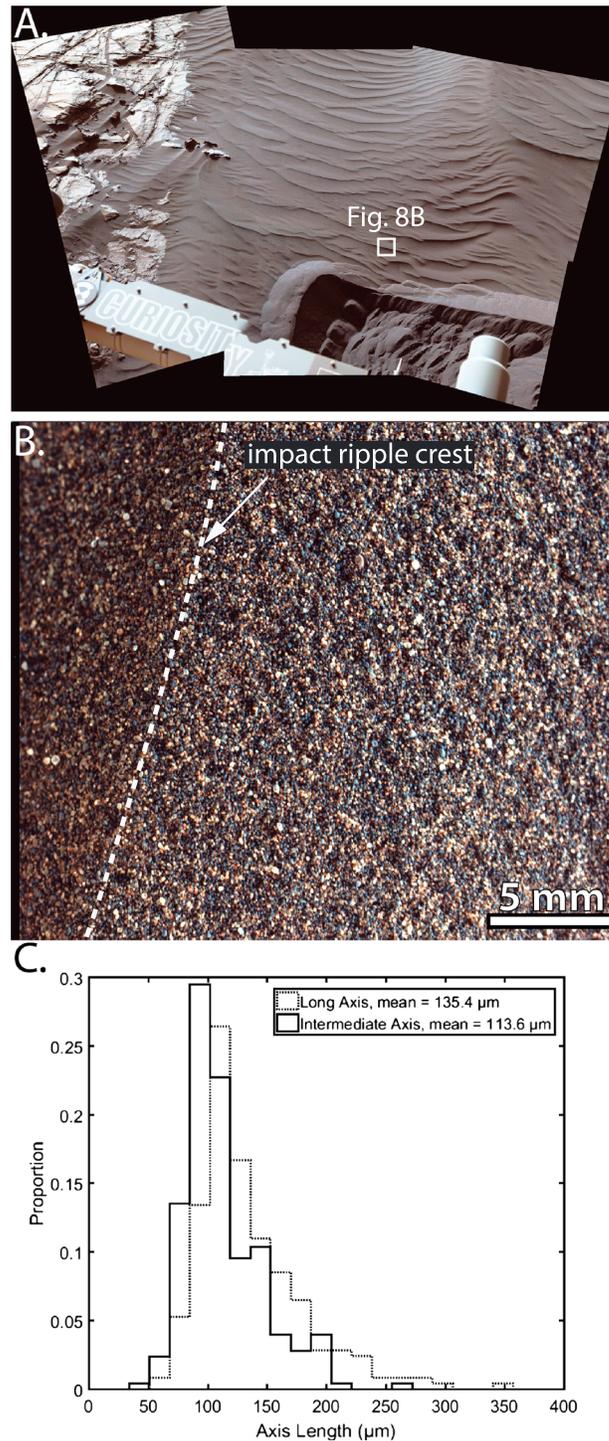
Figure 8. Impact ripple grain size distribution. (a) Mastcam image of target Otavi (white box) and the adjacent wheel scuff near Gobabeb. (b) 1 cm standoff MAHLI image of the undisturbed ripple Otavi. The spatial resolution is ~16 ± 0.2 μm per pixel. (c) Distribution of maximum and intermediate axis grain diameters at Otavi measured grid-by-number style. Note that the inset shown in Figure 8b is rotated clockwise by 90° from its position shown in Figure 8a. Images: mcam05599 (Figure 8a) and MAHLI image 1242MH0005620010403684C00 (Figure 8b).

77 m in length, 4.0 m high, and changed aspect by 43° between 183° and 226° azimuth. Slopes sampled between 20° and 35° have a mean of 27° with standard deviation of 4.6° (n = 485) (Figures 3b and 10a). A DEM generated from Mastcam images indicates an average lee slope gradient of 29°, which compares well with the HiRISE-derived slope values measured along the same transect (Figure 10b). Slope profiles from two HiRISE DEMs and the Mastcam DEM, all acquired at different times, show good agreement in the lower reaches of the slope but some divergence at the top of the slope (Figure 10c).

Sedimentary processes visible across the lee slope include large ripples, impact ripples, grainflow, and grainfall (Figure 11a). Mastcam images show a lateral transition in the distribution of impact ripples and grainflows with grainflows dominating the apex of the curvature of the slope and impact ripples dominating the horns (Figure 11a). Impact ripples on the lee slope have orientations parallel to the lee slope dip direction. Large-ripple crest lines also form on the lee slope at a wavelength ~ 10 times that of the impact ripples (Figures 11a and 11b). Figures 11a and 11b also show well-developed large-ripple crest lines near the dune brinkline with crest line orientations parallel to the dip direction of the lee slope and grainfall on the western face of the ripple. The large-ripple crest lines forming on the middle and upper areas of the dune lee slope appear to be exploiting the antecedent topography generated by grainflows.

A detailed Mastcam mosaic near the zone of maximum crest line curvature shows an Earth-like suite of lee slope sedimentary processes (Figures 12A and 12B). Most prominently, two grainflows make up the center of the lee slope at its apex in curvature. The grainflows extend from near the dune brinkline and have a typical amphitheater-headed scarp at their source, tapered center, and widened and thickened toe. The
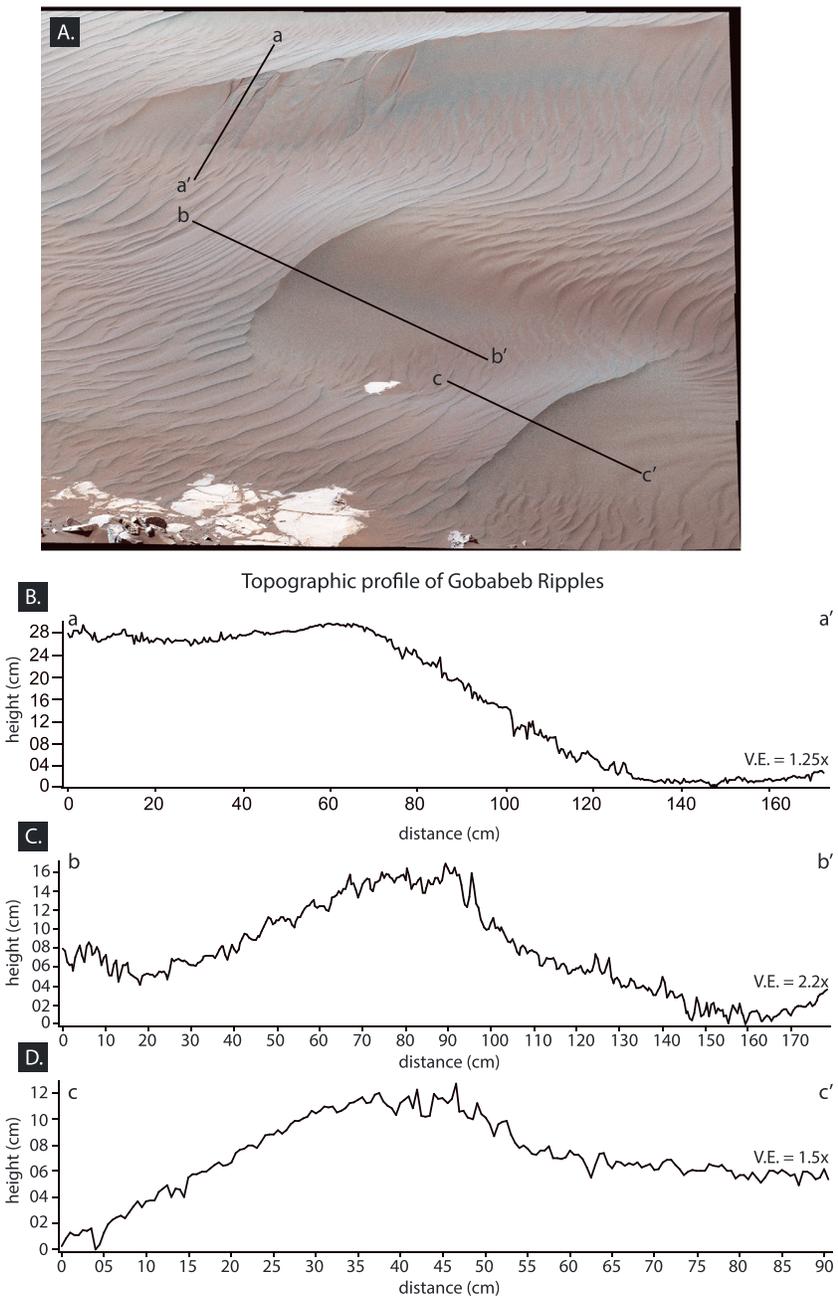
Figure 9. Mastcam image and topographic profiles from a DEM generated from Mastcam stereo of large ripples at Gobabeb. (a) Mastcam image showing part of Gobabeb shown in Figure 7 prior to wheel scuffing and scooping activity. The ripple in the background is the same as that shown in Figure 7a. The two ripples in the foreground are not visible in Figure 7. Note the difference in orientation between the large ripple in the background and the smaller, large ripples in the foreground. The large ripples in the foreground aligned with impact ripples, unlike the larger ripple in the background, which are oriented oblique to the impact ripples. (b) Topographic profile across the largest ripple in the background. The total height is ~28 cm. The stoss slope is nearly flat and the lee slope angle measures ~29° at its maximum slope. (c and d) Ripple profiles in Figures 9b and 9d are somewhat different from (Figure 9b) with steeper stoss slopes and over all lower slope angles. The high-frequency roughness of the topographic profiles arises from noise in the DEM generated by ranging errors (see methods for discussion). Images: mcam05597, Sol 1221 (Figure 9a).
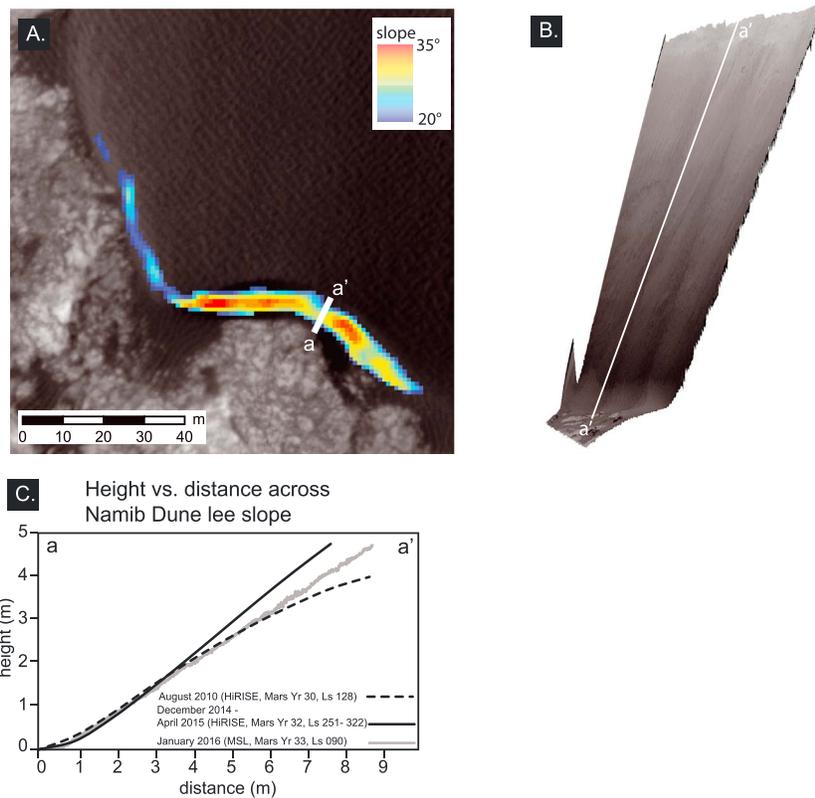
Figure 10. The lee slope of Namib Dune shown from (a) HiRISE image with an overlain slope map on the lee slope. The slope map is derived from a HiRISE DEM and values thresholded to a range between 20° and 35°. The thick white line shows the approximate location of Figure 9b and profiles shown in Figure 9c. (b) DEM derived from Mastcam images, thin white line indicates the profile shown in Figure 9c, and (c) a height profile comparing the slopes derived from the Mastcam and HiRISE DEMs. The slope profiles were fit to an origin of 0 m for comparison. Images: 2010 HiRISE DTM: DTEEC_018854_1755_018920_1755_U01 (1 m/pixel spatial resolution); 2015 HiRISE DTM: DTEEC_040770_1755_039280_1755_A01 (1 m/pixel spatial resolution); and HiRISE ESP_018854_1755 and HiRISE ESP_039280_1755 were used for dune and ripple measurements collocated with the 2010 and 2015 DEMs, respectively, but is not displayed, Mastcam image sequence: mcam05491, Sol 1198.

flows have several overlapping lobes, indicating that the several avalanches occurred within the same area. Adjacent to the flows, impact ripples with crest lines oriented parallel to the slip face overprint underlying palimpsest grainflows (Figure 12C). Horizontal fractures, scarps, and translational slides that occur within the rippled surfaces indicate that the underlying material is poorly consolidated and forming on near angle of repose slopes, consistent with measurements from the DEMs (Figure 10).

A small apron made up of impact ripples and large ripples intersected by grainflows defines the base of the dune. The origin of the apron is likely dune-generated grainfall that exceeded the length of the slip face and is now being reworked by large ripples and impact ripples. The large ripples in the dune lee are not as well defined as those on the stoss slope but have a similar wavelength at ~1.0 m. As elsewhere on the dune, the impact ripples contour and are influenced by the larger ripple topography. Grainfall characterizes the west facing slope of the large ripples and likely forms from large-ripple processes rather than grains overshooting the dune brinkline.

Large ripples occur at the brinkline of the dune (Figures 12A and 12D). Unlike typical dunes on Earth, this transition forms a variable slope break between the large ripples and the dune lee slope. The large ripples create a step-like morphology below which dune lee slope processes dominate (Figure 12D). Thus, the crest-to-brink transition on Martian dunes may be more akin to that of compound dunes (i.e., draas) on Earth in which superimposed dune migration over the crest, in part, controls lee slope dynamics, such as the size and location of grainflows.
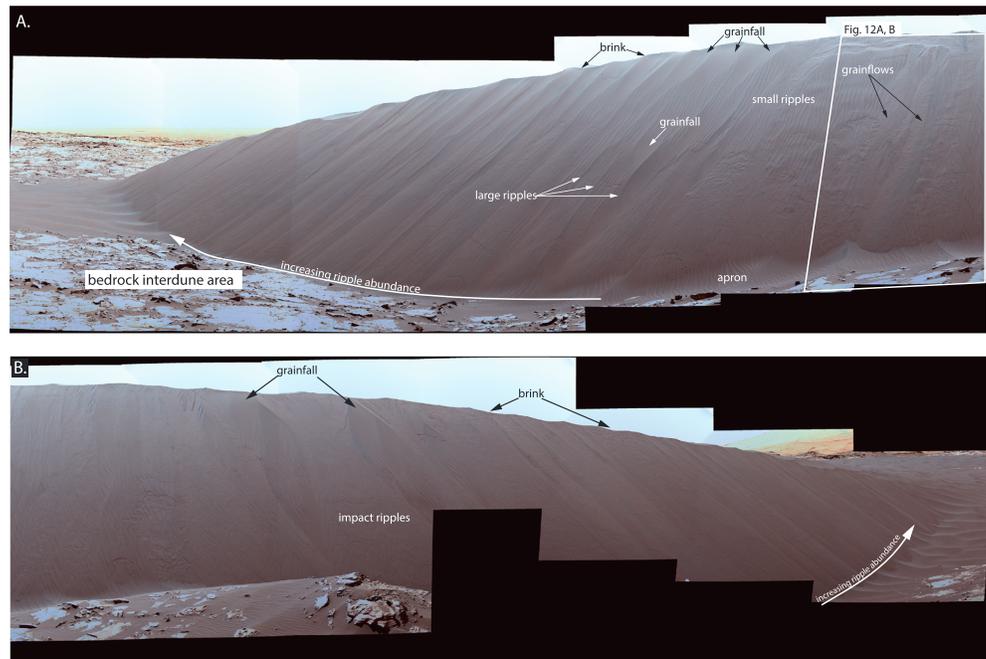
Figure 11. Lee slope of Namib Dune. (a) Left and (b) right halves of a Mastcam mosaic showing the distribution of grainfall, grainflow, small impact ripples, and large ripples forming across the lee slope. Note the increasing amount of wind ripple cover toward the horns of Namib Dune. Large ripples appear in the middle of the lee slope along with impact ripples implying that they are forming coincidently. Some grainflow scarps appear to be developing into large-ripple topography near the brink area. The western flanks of large ripples are covered in grainfall and imply along-slope transport from the east. Images: mcam05504, Sol 1201 (Figures 11a and 11b).

The secondary lee slope of Namib Dune is dominated by large ripples migrating obliquely down the slope toward the south and the central horn of the dune that defines the intersection of the primary and secondary lee slopes (Figure 13A). The secondary lee slope as measured from a HiRISE DEM has a mean slope of 16° (standard deviation: 5°; $n = 355$) with a maximum up to 34° near the horn of the dune. The height and length are 2.5 m and 60 m, respectively. Notably, sedimentary processes on the secondary lee slope are defined by large ripples migrating down the slope rather than by processes that dominate on the primary lee slopes, such as grainflow and grainfall. This is consistent with the overall lower slopes and a gradual brink-to-lee slope transition in which airflow moving over the dune would remain attached to the surface. The large ripples on the secondary lee slope have a straighter, less sinuous (e.g., two-dimensional) crest morphology in plan view than large ripples found elsewhere on the dune. The less sinuous nature of the ripple may be related to their formation on a slope in which lateral diffusion of the sinuosity could occur through grain avalanches that flow down the vector component of the ripple lee slope and the secondary lee slope (Figure 13B) [*Rubin*, 2012].

Other than the two-dimensional nature of the large-ripple crest lines on the lee slope, they have morphologic features that are similar to those at Gobabeb. Impact ripples contour around and over the large ripple before giving way to lee slope processes. The lee slope processes are defined by grainflows, grainfall, and fractures that generate typical and translational grainflow slides down the lee slope. A Mastcam DEM shows that the overall slope of the secondary lee slope is 23°, which compares well with the HiRISE DEM, and that areas of grainfall occur at 32°–33°, with an outlier of 40°, and angles measured across the grainflows are at 29° (Figure 13B).

4.3. Interdune Area

The interdune area on which Curiosity drove between High Dune and Namib Dune is wind-sculpted and eroded bedrock covered by sparse sand patches and loose pebble- to boulder-sized rocks. The exposed surfaces denote a sediment availability-limited system in which limited sand supply contributes to the overall Bagnold Dune transport system (Figure 14a) (see discussion in *Lapotre et al.* [2017]). Wind abrasion features within the interdune area include fluting (Figures 14a and 14b). White veins interpreted as calcium sulfate as
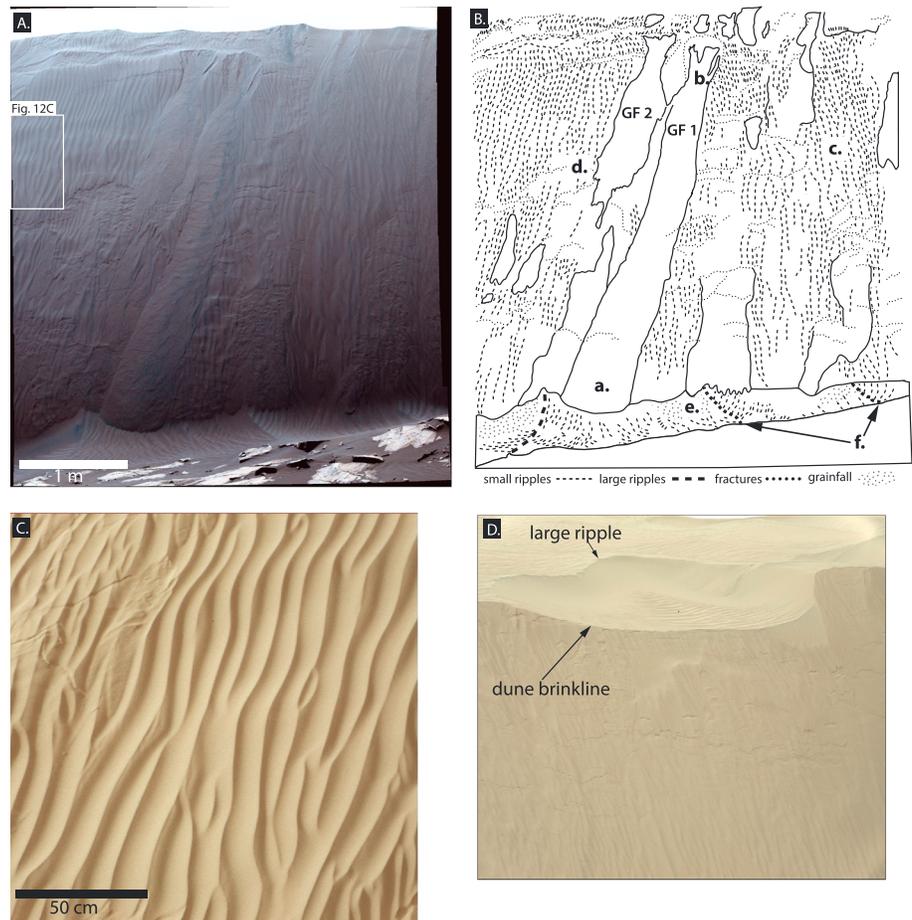
Figure 12. Mastcam mosaic and images of the central portion of the Namib Dune lee slope. (A) Mastcam mosaic and (B) digitized sedimentary processes. (a) grainflow lobe; (b) grainflow scarp; (c) impact ripples; (d) fractures; (e) grainfall; (f) large ripples; and (e and f) dune basal apron. (C) Mastcam image of the impact ripples on the lee slope. The asymmetry of the impact ripples is not clear and wind flow direction cannot be determined from these structures alone. (D) Brinkline of Namib Dune showing the "double-step" morphology from the migration of large ripples over the brink. Images: mcam05491, Sol 1198 (Figure 12A); mcam05508, Sol 1201 (Figure 12C); and mcam05449, Sol 1196 Figure 12D.

imaged at High Dune [*Elhmann et al.*, 2017] occur within the interdune area (Figure 14b) and likely are the source of the coarse grains that collect within the grainflows at Gobabeb (Figure 7). This indicates that sand generated from abrasion is at least a partial sand source for the modern dune system. The most prominent sand feature of the interdune area is a set of large ripples emanating from the horn of Namib Dune at the intersection of the primary and secondary lee slopes (Figure 14c). Large, straight-crested, two-dimensional ripples extend parallel to one another toward the west-southwest before dissipating into interdune bedrock. The ripples are covered by smaller ripples, which are oriented nearly transverse to the crests of the large ripples.

5. Interpretation of Sedimentary Processes of the Namib and High Dunes

5.1. Ripples

Observations from Curiosity's traverse through the Bagnold Dunes demonstrated that Martian dunes host two scales of ripples [*Lapotre et al.*, 2016]. The large ripples have been recognized from orbit [e.g., *Bridges et al.*, 2007], and the smaller ones were discovered on dunes for the first time upon arrival to the Bagnold Dunes [*Lapotre et al.*, 2016]. Whereas the low-relief profiles and straight-crested planform geometry of small ripples are typical of wind impact ripples, the larger ripples, with sinuous crests and angle of repose slopes, are unlike any wind-blown ripples that develop on dunes on Earth [*Lapotre et al.*, 2016].
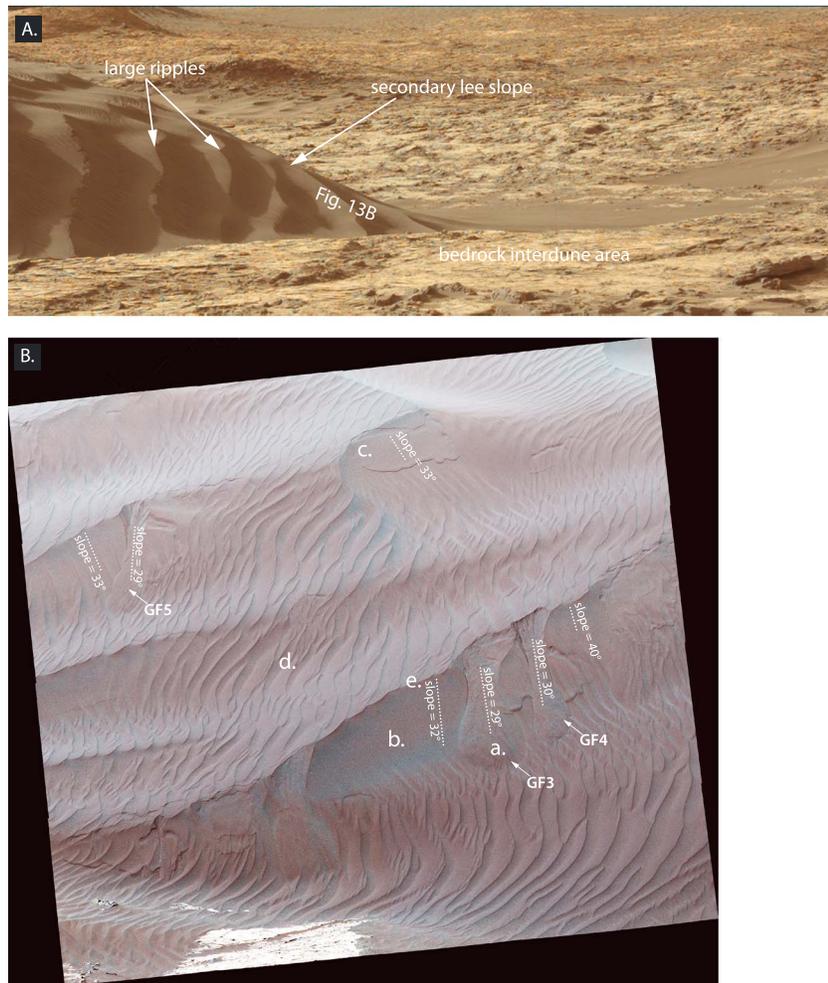
Figure 13. Mastcam images of secondary lee slope of Namib Dune. (A) Mastcam image taken from interdune area showing the large ripples migrating obliquely down the secondary lee slope toward the east-southeast. (B) Mastcam image showing sedimentary structures on large ripples. The lowercase white letters refer to (a) grainflow, (b) grainfall, (c) fracture and slide on large-ripple lee slope, (d) impact ripples, and (e) large-ripple brink. Measurements from a Mastcam stereo DTM are shown on the grainflow and grainfall areas of the ripple. Note that the grainflows are consistently lower in slope than the grainfall. The grainflows are avalanching at an oblique, rather than transverse angle to the crest line. The avalanches follow the downslope direction of the combined dune and ripple slopes and may reduce the sinuosity of the large ripples [e.g., *Rubin*, 2012]. mcam05410, Sol 1192 (Figure 13A); mcam05418, Sol 1194 (Figure 13B).

Lapotre et al. [2016] applied the term "wind-drag" [cf., *Bagnold*, 1941] ripple to the large ripples as a reference to the apparent important role played by fluid viscosity on ripple size and stability [e.g., *Southard and Boguchwal*, 1990; *Lapotre et al.*, 2017]. Two main ways by which viscosity was proposed to come into play are through the thickness of the laminar sublayer [e.g., *Yalin*, 1985] or through the turbulence of the wake past the bed form crests [e.g., *Bennett and Best*, 1995].

Though their precise formation mechanism is not well understood, the large ripples do not appear to be coarse-grained ripples or large impact ripples [*Lapotre et al.*, 2016]. *Lapotre et al.* [2016, Figures 1e and 1f] show MAHLI images of the crest of a large ripple in which no discernable grain size variation is visible between the crest and the slopes of the ripple. Our Figure 8 shows that the grain size distribution of the undisturbed grains on an impact ripple at Gobabeb ranges between 50 μm and 350 μm with an average, intermediate axis size of 113 μm. No discernable difference between the body of the ripple and the crest is visible, and the grains are similar in size to grains in an adjacent wheel scuff (~80–350 μm diameters) [*Elhmann et al.*, 2017]. The grain size similarity between the undisturbed ripple and the nearby wheel scuff indicates that surface and bulk grain sizes are similar at Gobabeb. This supports the conclusions of *Lapotre*
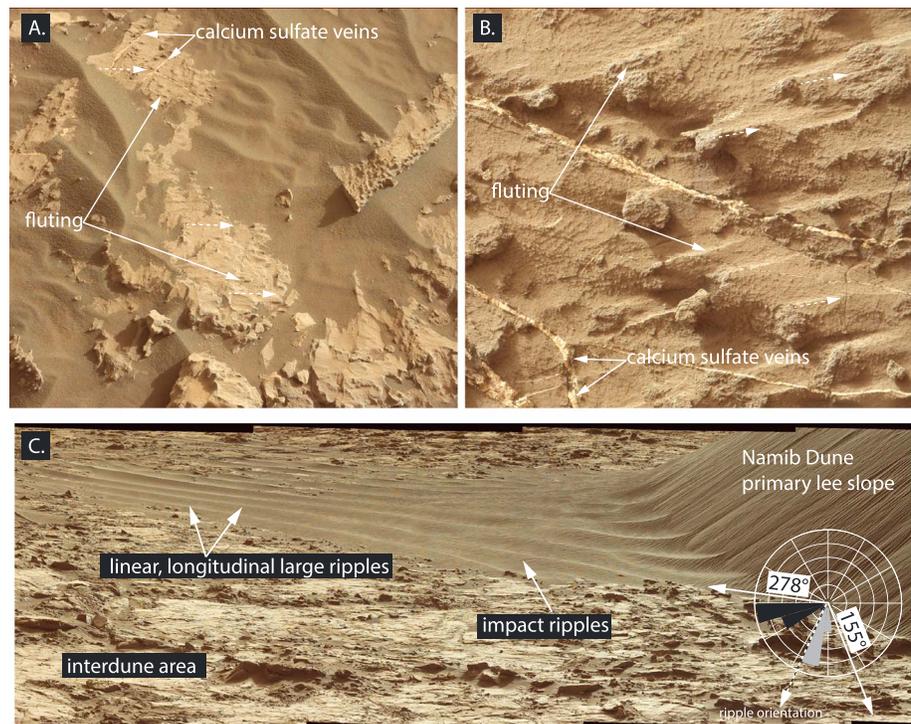
Figure 14. Mastcam images showing interdune area between High Dune and Namib Dune. (a) Wind sculpted bedrock making up sediment availability-limited interdune surface. (b) Wind abraded bedrock showing flute structures. (c) Linear large ripples formed at the intersection of the primary and secondary lee slopes of Namib Dune. Note the small ripples migrating orthogonal to the orientation of the linear ripple. The rose diagram shows the dip directions of the primary lee slope (gray) and secondary lee slope (black). The solid white arrows indicate the along-slope sand transport direction from each slope where 278° corresponds to the direction of transport on the primary lee slope and 155° corresponds to the direction of transport on the secondary lee slope. The dashed white arrow indicates the orientation of the large ripples, which bisects the along slope transport directions. Images: mcam05330, Sol 1176 (Figure 14a); mcam05501, Sol 1200 (Figure 14b); and mcam05520, Sol 1214 (Figure 14c).

et al. [2016] that the large ripples at Gobabeb formed within a unimodal grain size distribution and not from a strongly bimodal grain distribution as would be the case for coarse-grained ripples.

Evidence against an impact-ripple mechanism for the large ripples beyond that discussed in *Lapotre et al.* [2016] includes the similar orientation of the large and impact ripples shown in Figure 9. The impact ripples in Figure 9 are oriented parallel to the large ripples shown in Figures 9c and 9d, which implies that these large ripples formed coincident with the surrounding impact ripples or, as discussed below, were reoriented to the same orientation. In both cases, the large ripples remained stable through impact ripple movement, and no current model of wind impact ripple formation can generate two superimposed stable wavelengths of impact ripple [*Durán et al.*, 2014]. If the large ripples shown in Figures 9c and 9d are incipient forms of the larger, large ripples (e.g., Figure 9a), this may explain their somewhat different topographic profiles (Figures 9c and 9d). The large-ripple profiles, while asymmetric, have overall shallower lee slopes, which would be consistent with nascent bed forms (e.g., protodunes). In this case, these ripples would be proto-large ripples that exhibit the transition toward developing an angle of repose slip face similar to their larger counterparts. This also implies that the ~1 m wavelength is near the emergent wavelength. One meter is also consistent with the scale of the large-ripple crest lines beginning to develop on the lee slope of Namib Dune (Figure 10).

Different from the large ripples at Gobabeb (Figure 9) and at the secondary lee slope of Namib Dune (Figure 13), the large ripples that occur at the base of the stoss slope of High Dune have coarser-grained crests, a more symmetric topographic profile, greater wavelengths, and an overall brighter appearance (Figure 5). The grain sizes measured near "Barby" targeted on Sol 1184 range between ~150 and 600 μm, which is a wider range and coarser than that measured at the ripple Otavi (Figure 8) [*Elhmann et al.*, 2017].

The large ripples at the base of High Dune are most similar to the large, coarse-grained ripples identified by *Sullivan et al.* [2008] at the El Dorado ripple field in Gusev crater and more typical of coarse-grained ripples on Earth [*Sharp*, 1963; *Yizhaq et al.*, 2012]. Their position at the base of High Dune likely arises because of spatial sorting between the coarser and finer fractions of the sediment supply. Whereas the fine fraction is mobilized into the dune, the coarser fraction remains at the base as a lag deposit, which renders the ripples relatively immobile under current conditions [e.g., *Lapotre et al.*, 2017]. The grain size contrast and commensurate increased stability probably accounts for the greater brightness compared to other large ripples upslope on High Dune. Given the juxtaposition of coarse-grained ripples and typical large ripples on High Dune's stoss slope, some potential process relationship is implied, yet remains unknown (e.g., the different ripple types may represent two distinct formative mechanisms or a single mechanism in which the large-ripple instability creates a template for the coarse-grained ripples).

5.2. Relating Wind to Spatial Variations in Sedimentary Processes on the Lee Slope of Namib Dune

The type and distribution of sedimentary processes on a dune are strongly affected by dune shape [*Sweet and Kocurek*, 1990; *Wiggs et al.*, 1996; *Eastwood et al.*, 2012]. On the lee slope, the distribution of processes reflects the instantaneous magnitude and direction of the wind with respect to the local crest line orientation, which is known as the incidence angle [*Sweet and Kocurek*, 1990; *Walker and Nickling*, 2002; *Eastwood et al.*, 2012; *Pelletier et al.*, 2015; *Swanson et al.*, 2016]. Given a range of crest line curvatures and wind directions, the processes on a lee slope are expected to vary spatially and temporally related to the fluid dynamics of dune-modified secondary flows [*Tsoar*, 1983; *Sweet and Kocurek*, 1990; *Walker and Nickling*, 2002; *Eastwood et al.*, 2012]. Field and laboratory studies show that flows that strike a crest line with incidence angles between 70° and 90° generate a two-dimensional eddy in the recirculation zone that promotes gravity-driven deposition on the lee slope such as grainflow and grainfall. At lower incidence angles, an along slope three-dimensional vortex develops that generates both gravity driven and traction transport and results in the progressive transition from grainflows with wind ripple bottom sets (70°–40°) to fully wind ripple covered surfaces (40°–25°). At yet lower incidence angles when the wind is blowing nearly parallel to or toward the slip face, <25°, bypass and erosional reactivation surfaces develop. Given the reasonably tight control on the relationship between incidence angle and sedimentary processes, the distribution of sedimentary processes can be used inversely to point to the formative winds [*Ewing et al.*, 2010; *Eastwood et al.*, 2012].

Spatial variations of sedimentary processes across Namib Dune primary and secondary lee slopes and the ripples at Gobabeb imply recent changes in the winds (Figures 7, 11, and 12). The Mastcam mosaic of Namib Dune shown in Figure 12 shows fresh grainflows occurring at an aspect of 202° near the point of maximum curvature of the dune. The aspect of the primary lee slope ranges between 183° and 226° and the secondary lee slope between 280° and 230°. Based on the ubiquitous impact ripple coverage on both lee slopes and the incidence-angle zones given above, recent winds that formed the structures were unlikely to be from between 320° and 90° clockwise azimuth. Winds within this zone would have been sufficiently orthogonal to the Namib Dune crest line to generate more widespread, unrippled, grainflows than observed. Winds from between the southeast and west-northwest clockwise azimuths could account for the presence of impact ripples on the slip faces.

Although, any single wind within the range of possible winds would be sufficiently oblique or longitudinal to generate impact ripples, the ripple orientations and other structures on the different slopes indicate that two winds were acting on the dune. Based on the presence of grainfall on the westward side of the incipient large ripples along the slip face and at the base of Namib Dune [Figures 10a and 11a], the most recent winds at the time of observation affecting the primary lee slope were likely from the southeastern quadrant. Any southeasterly wind would deposit grainfall on the west-facing lee slope of the large ripples. On the secondary slip face, the large and small ripples all appear to be oriented to a westerly or west-northwesterly wind. Westerly winds are also consistent with the asymmetry of the High Dune ripple and the presence of grainfall in the east-facing lees of High Dune ripples. These estimates compare well to the possible winds proposed to generate the ripple and dune distribution in the Bagnold Dune Field [*Silvestro et al.*, 2013; *Day and Kocurek*, 2015], wind reconstructions from REMS data and models [*Newman et al.*, 2017], and observations of grain motion [*Bridges et al.*, 2017], all of which indicate both westerly and easterly winds. The cooccurrence of opposing ripple orientations on the dune implies that the dune slopes shield parts of the dune from some components of the wind regime, consistent with REMS data [*Newman et al.*, 2017]. Although REMS data collected at the

primary lee slope of Namib Dune indicate westerly winds, these winds do not appear to have strongly affected the slope. Because of the orientation of the rover, easterly wind directions could not be measured, but high wind speeds were detected during the evening putatively easterly winds [*Newman et al.*, 2017]. Given the presence of palimpsest grainflows across the lee slope and the overall shape of the dune, it is unlikely that the recent winds that modified the dune are the dominant transporting winds responsible for the bulk of the dune shape or dune migration. The shape more likely reflects dominant north-northwesterly winds that would generate grainflows.

5.3. Angles of Repose on Namib Dune

The angle of repose is defined by the maximum slope at which granular material rests [*Allen*, 1970; *Lowe*, 1976]. Although this is thought to be primarily controlled by the properties of the granular material (e.g., angularity and roughness) [*Carrigy*, 1970], the role of lower gravity on the angle of repose has been the subject of some controversy and may have implications for bed form dynamics and the rock record on Mars [e.g., *Kleinhans et al.*, 2011]. In reduced-gravity experimental tests done during parabolic flights, grain avalanches were recorded under different accelerations [*Kleinhans et al.*, 2011]. *Kleinhans et al.* [2011] found that at 0.1 g acceleration the static angle of repose (i.e., the angle to which grains can build before avalanching and also known as the angle of initial yield or critical angle) increased by 5° and the dynamic angle of repose (i.e., the angle at which avalanches come to rest, also known as the relaxation angle) decreased by 10°. As a consequence of the effects of gravity, *Kleinhans et al.* [2011] suggested that the size of the avalanches would also increase. Their results at Martian gravitational accelerations showed that differences from Earth would be minimal for static angles of repose but might vary by ~5° for dynamic angles of repose. Potential problems with the reliability of the outcomes arise because the study was conducted in flight with little control on changing accelerations during flight or vibrations that might have caused the avalanching to behave differently. In another study, *Atwood-Stone and McEwen* [2013] determined the lee slope angle on Martian sand dunes using HiRISE DEMs. They found that angles ranged between 29° and 35°, which is within the range of expected angle of repose for dunes on Earth [*Allen*, 1970; *Lowe*, 1976; *Kleinhans*, 2004, *Sutton et al.*, 2013] and consistent with other measurements of lee slope angles on Mars [*Silvestro et al.*, 2013; *Cardinale et al.*, 2016].

The presence of fresh grainflows and the abundance of palimpsest grainflows on the lee slope of Namib Dune points to the expected aerodynamics in the lee of a dune in which flow across the brinkline separates, which allows grains mobilized over the brink to settle out onto the lee slope as grainfall. Although no primary grainfall was present on the dune lee slopes, widespread grainfall on the slope is implied by the presence of grainflows, which initiate as a buildup of grainfall to the static angle of repose. The grainfall buildup relaxes into a grainflow that represents the dynamic angle of repose. Thus, the majority of Namib Dune's primary lee slope reflects an angle near the dynamic angle of repose.

A Mastcam DEM of the lee face of Namib Dune shows the average slope from brink-to-base to be 29°, which is within the range of the dynamic angle of repose measured by *Atwood-Stone and McEwen* [2013], determined for Earth [e.g., *Allen*, 1970, *Sutton et al.*, 2013], and measured by HiRISE for Namib Dune (Figure 8). The DEM was not sufficiently resolved because of the range from Mastcam to the dune to measure centimeter-scale areas of the Namib Dune slip face, which prevented a comparison between the slopes of the grainflows and the wind rippled areas. The presence of impact ripples on the lee slope indicates that the slope is below the angle of repose, but the widespread presence of fractures, some of which have triggered grainflows, indicates that the slope is likely to be close to its natural angle of repose.

Although detailed topographic measurements of grainflows on the Namib Dune lee slope were not feasible with the Mastcam DEMs because of the large ranging distance of Mastcam from the lee slope, measurements of the width of the theater-headed scarp and the grainflow lobe at the toe were gathered using the orthoimages (Table 1). The scarps and lobes are somewhat larger than those measured on a barchan dune of similar size on Earth [cf., *Nield et al.*, 2017]. The Martian grainflows are more similar in size to grainflows generated on an experimental dune that was 4 times smaller than Namib Dune [*Sutton et al.*, 2013]. This difference likely arises from the statistically insignificant sampling, but feasibly could also relate to differences in grain shape that result from the diverse mineralogy of the Bagnold sands [*Achilles et al.*, 2017], differences in gravity [*Kleinhans et al.*, 2011], or release of rarefied gas through the porous sand [*Schmidt et al.*, 2017].

Table 1. Comparison of Terrestrial and Martian Grainflow Characteristics From Field and Laboratory Studies[a]

Planet	Location	Bed Form Type	Measurement Type	Author	Scarp Width (m)	Scarp Length (m)	Lobe Width (m)	Lobe Length (m)	Thickness (m)	Static Angle of Repose (deg)	Dynamic Angle of Repose (deg)
Earth	Namibia	dune	field	*Nield et al.* [2017]	0.23	0.4	0.3	1.19	0.0149	36.6	31.9
Earth	Brazil	dune	field	*Pelletier et al.* [2015] (see Figure 11a – large dune)			no data			32.27	32.16
Earth	Brazil	dune	field	*Pelletier et al.* [2015] (see Figure 11b – small dune)						32.48	32.15
Earth	Canada	dune	experimental	*Sutton et al.* [2013] (see Figure 4; row 1, column 1)	0.54	0.58	0.71	1.25	no data	34	32
Earth	Canada	dune	experimental	*Sutton et al.* [2013] (see Figure 4; row 1, column 2)	0.63	0.7	0.8	1.14		34	32
Earth	Canada	dune	experimental	*Sutton et al.* [2013] (see Figure 4, row 2, column 1)	0.58	0.72	0.71	1.06		34	32
Mars	Gale crater, Namib Dune	dune – primary lee slope	field	dune grainflow (Figure 12 – GF1) (mcam05491)	0.67	1.6	0.66	6	no data	no data	29
Mars	Gale crater, Namib Dune	dune – primary lee slope	field	dune grainflow (Figure 12 – GF2) (mcam05491)	0.54	1	0.57	2.9			29
Mars	Gale crater, Namib Dune	large ripple on secondary lee slope	field	large-ripple grainflow (Figure 13 – GF3) (mcam05418)	0.43	0.25	0.32	0.81		32	29
Mars	Gale crater, Namib Dune	large-ripple on secondary lee slope	field	large-ripple grainflow (Figure 13 – GF4) (mcam05418)	0.3	0.13	0.19	0.96		40	30
Mars	Gale crater, Namib Dune	large ripple on secondary lee slope	field	large-ripple grainflow (Figure 13 – GF5) (mcam05418)	0.16	0.19	0.17	0.96		33	29

[a]The values reported in this study were acquired from orthorectified images generated through the Mastcam DEM process using GIS. The images had a spatial resolution of 2–5 mm/pixel. Uncertainty in the measurements arises from identifying the boundaries of the grainflow characteristics and is estimated at 3–4 times the spatial resolution of the image and thus a maximum of ± 8–20 mm per measurement. Measurements acquired in this study are highlighted in gray.

On the secondary lee slope of Namib Dune, a detailed DEM generated from Mastcam imaging allowed for the measurement of angles across the entire slope and on different slopes of the large ripples. The average over the secondary lee slope where measured by Mastcam measured 23°. Grainfall areas of the ripples measured 32° and 33° with an outlier of 40°. These angles are interpreted to approximate the static angle of repose based on the adjacent grainflows. The outlier of 40° may indicate some material cohesion within the sediments that would allow a higher angle static angle of repose. An additional cohesion mechanism would be consistent with fractures formed on the ripple and dune lee slopes (Figures 11–13). Grainflows had a slope of 29°, which is taken as the dynamic angle of repose. Measurements of ripple profiles from Gobabeb support the 29° dynamic angle of repose (Figure 7). As with the Namib Dune primary slip face, the angles measured on the ripples fall within a typical terrestrial range of lee slope angles (Table 1). Overall, using both HiRISE and Mastcam DEMs, we observed no significant differences between angles of repose on Martian bed forms and those reported for Earth.

5.4. Large-Ripple and Dune-Field Pattern Development

On Earth, dune-field and ripple-field patterns develop through different fundamental mechanisms, at different spatial scales, and within different boundary conditions and can be treated as separate pattern-forming processes [*Ewing et al.*, 2015]. For example, ripples forming on the stoss slope of a dune may develop in transport-limited conditions, whereas the host dune may be forming within sediment availability-limited conditions. Ripple patterns may be in a well-organized, mature state even when a dune-field pattern is in its infancy. A comparative approach between the scales, however, can yield information about the formative conditions not accessible by analysis of one of the scales alone [*Ewing et al.*, 2010; *Ewing et al.*, 2015]. The relevant bed form pattern scales for interpreting boundary conditions in the Bagnold Dune Field are the impact ripples, large ripples, and dunes.

The linear, longitudinal large ripples formed in the interdune area at the intersection of the primary and secondary lee slopes on Namib Dune demonstrate that the large-ripple patterns on Mars reflect an integrated wind signal. This observation substantiates observations of linear, longitudinal large ripples formed on the linear dunes that make up the center and western flank of the Bagnold Dune Field [*Silvestro et al.*, 2016; *Vaz et al.*, 2016]. Though this pattern-forming behavior has long been understood, recognized, and employed in the analysis of sand dunes on Earth, Mars, and Titan, ripples have been thought to be reliable indicators of the instantaneous flow direction of the last transporting wind [*Rubin and Hunter*, 1987; *Sweet and Kocurek*, 1990; *Rubin and Hesp*, 2009; *Ewing et al.*, 2010; *du Pont et al.*, 2014; *Jackson et al.*, 2015]. This thinking arose because impact ripples on Earth are small bed forms and quick to reorient to most transport events. Rapid reorientation occurs because the magnitude and duration of sand transport events on Earth typically exceed the time needed to reform or reorient the ripples. Restated, impact ripples on Earth are volumetrically small relative to the sand fluxes associated with the magnitude and duration of a typical transporting wind event. On Mars, however, because the large ripples appear to integrate the wind signal, typical transporting wind events must move a relatively small fraction of the total ripple volume such that the large ripples are not reformed and persist in a stable orientation. Thus, the large-ripple crest lines are therefore expected to orient to gross bed form normal transport or fingering-mode orientation with respect to multiple winds in an overall wind regime [*Rubin and Hunter*, 1987; *du Pont*, 2014; *Swanson et al.*, 2016; *Silvestro et al.*, 2016].

Ripples forming in the interdune area at the horn of Namib Dune can be explained as linear, longitudinal ripples formed by converging along-slope sand transport toward 278° and 155° from the primary and secondary lee slopes, respectively (Figure 14c). Based on the inferred along-slope transport directions, flows arriving at this point from the two slopes are separated by a divergence angle of 123°, which is within the expected range for longitudinal and oblique bed form development [*Rubin and Hunter*, 1987]. This interpretation is consistent with their strikingly two-dimensional morphology [*Rubin*, 2012] and the presence of smaller ripples migrating orthogonally along their crest [*Rubin and Hunter*, 1985].

The cross-hatch ripple pattern that dominates the stoss slope of High and Namib Dunes points to the presence of two primary winds within the dune field with modification from stoss-slope topography. Unlike the linear, longitudinal ripples formed within the interdune area, the cross-hatch ripple pattern indicates that the ripple patterns may be partially reformed and overprinted during different wind events such that each crest line orientation represents discrete components of the wind regime or that the crest line pattern is integrating winds with a divergence angle of around 90° [*Dalrymple and Rhodes*, 1995; *Werner and Kocurek*, 1997;
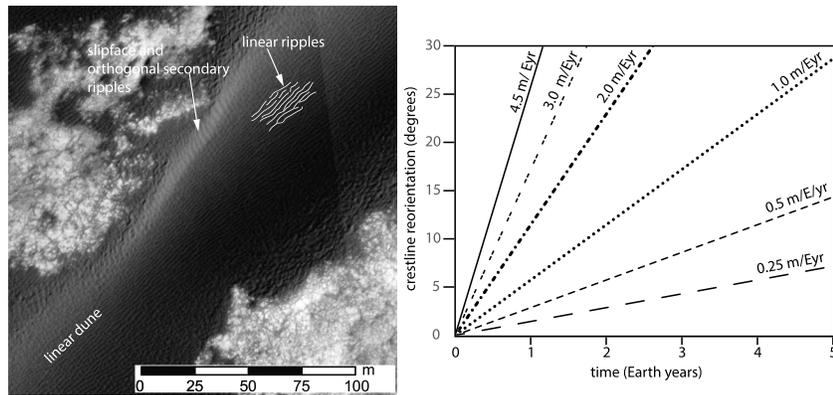
Figure 15. HiRISE image of the linear dune area of the Bagnold Dune Field and a plot of ripple reorientation rates. (a) HiRISE image showing linear longitudinal ripples analyzed by *Silvestro et al.* [2016]. Note the secondary ripples migrating along a slip face of the linear dune are orthogonal to the orientation of the ripples at the crest. (b) The degree of ripple reorientation for different ripple migration rates. The timescales are based on *Werner and Kocurek* [1997] model of bed form reorientation through defect migration. Plot of the time to reorient a 10 m long ripple by varying degrees for different ripple migration rates. Images: HiRISE image: ESP_018854_1755_RED.

Reffet et al., 2010]. Mastcam images of grainflows demonstrate that both crest lines remain active during the wind regime cycle (Figure 6), though one crest line orientation is likely more active than the other during different parts of the wind cycle. At a yet larger scale, the predominance of the cross-hatch pattern at the dune crests across the dune field may arise because of the stoss-slope wind speed-up effect, in which winds not sufficient to mobilize grains on the lower part of the dune and within the interdune area, generates stress sufficiently large to mobilize sand at the crest and thus the crests would be subject to a greater distribution of winds within a wind regime [*Gao et al.*, 2015].

In contrast to the cross-hatch ripple pattern in the barchan dune area of the Bagnold Dune Field, a striking field-scale example of linear, longitudinal ripples occurs in the linear dune area of the Bagnold Dune Field (Figure 15a) [*Silvestro et al.*, 2016]. The dunes in this area have two opposing slip faces and have a sinuous, seif-dune appearance. These have been referred to as linear, longitudinal dunes, and their morphology is consistent with modeled winds of Gale crater [*Hobbs et al.*, 2010; *Silvestro et al.*, 2013; *Day and Kocurek*, 2015; *Newman et al.*, 2017]. Superimposed upon these dunes are large ripples with crest lines oriented axis-parallel to the orientation of the linear dune [*Silvestro et al.*, 2016]. Ripple migration mapping in this area revealed that the ripple bifurcations are moving along the axis of the dune consistent with the linear, long-itudinal ripple migration [*Silvestro et al.*, 2016]. Further evidence for the linear longitudinal ripple pattern is provided by the secondary ripples formed on the north facing lee slope of the linear dune, which are ortho-gonal to the dominant dune and ripple orientation. This likely arises from secondary flows deflected across the dune crest as would be expected from either a northeasterly or northwesterly flow (Figure 15a).

In the linear dune area of the Bagnold Dune Field, the persistent uniformity between the ripple and dune orientation implies that the formative winds for both the dunes and the ripples are occurring over timescales with cycles too short to alter the long-term orientation. The maximum timescale for the wind cycle for both bed forms can be approximated by estimating the maximum amount of time needed to reorient a ripple. For example, given a large-ripple migration rate of 1.7 m/Eyr (i.e., Earth year) [*Silvestro et al.*, 2016] and a mean crest line length of 10 m, the timescale to reorient the large ripples by 20° based on the *Werner and Kocurek* [1997] model is about 2 Earth years (Figure 15b). The winds that do work on the ripples could cycle on any timescale shorter than two Earth years and be integrated into a ripple orientation that remains unmo-dified by less than 20°. The most likely wind cycles occur on seasonal and diurnal timescales, which are shorter than 2 Earth years [*Newman et al.*, 2017]. The timescale to reorient ripples across the field will vary depending on the length and migration rate of the ripples, and if new crest lines develop and rework the ripples, the rates would be somewhat higher [*Werner and Kocurek*, 1997]. Figure 15b shows a range of reor-ientation times and angles for a 10 m long ripple for different migration rates based on a range of measured migration rates across Mars and in Gale crater [*Bridges et al.*, 2012; *Silvestro et al.*, 2013; *Cardinale et al.*, 2016]. Given the range of crest line lengths within the ripple field, smaller ripples at higher migration rates could

reorient on a monthly timescale. At Gobabeb, the ~80 cm long ripples shown in the foreground of Figure 9a are migrating at ~0.5 m/yr [*Lapotre et al.*, 2017; *Bridges et al.*, 2017] and could reorient 20° in 2 months.

As with the comparison between the large ripples and dunes, if the large ripples are consistent in orientation to the small ripples, it is the reorientation timescale of the smallest ripple that reflects the formative wind cycle of both scales of bed forms. Relative reorientation rates may explain the consistent orientation between the smallest large ripples and the impact ripples and the difference in orientation between the smallest, large ripples and the largest ripples observed at Gobabeb (Figures 7 and 9). At Gobabeb, impact ripples are aligned parallel to the 80 cm long large ripples and the largest, large ripples are oriented obliquely to the 80 cm large ripples. Thus, the 80 cm large ripples have formed under the same wind regime as the smallest impact ripples, but the largest large ripples have not been substantially reoriented during the same time period. A shift in winds to the direction inferred from the small ripple orientation explains the reoriented defect observed in Figures 7 and 9a and is consistent with the activity of both crest line modes shown in Figure 6. The diurnal, westerly, and easterly winds implied by models, grain transport, and morphologic indicators (Figure 12) [*Bridges et al.*, 2017, *Newman et al.*, 2017] may be part of a consistent, months long, seasonal wind regime as indicated by the reorientation rates and observations of similar and differently oriented scales of ripple (Figures 9 and 15). These examples serve to highlight the resilience of the large ripples to modification under the current climate conditions and show that sand fluxes would have to be much greater than are currently estimated to modify significantly the largest ripples during the course of a single wind event as occurs on Earth.

6. Implications of Bagnold Dune Field Sedimentary Processes for the Eolian Stratigraphic Record of Mars

Cross stratification is a temporal record of lee-face deposition arising from bed form migration. Curiosity's traverse through the Bagnold Dune Field revealed similarities and differences between lee face processes on Earth and Mars that should manifest within Mars' stratigraphic record. The formation of large ripples is the most notable difference from Earth, but the manifestations of grainflow, grainfall, and impact ripples are similar. These processes and the way in which these processes interact with the dune lee slope are expected to generate a uniquely Martian stratigraphic signature of bed form migration that is outside the bounds of an Earth analog.

6.1. Large-Ripple Stratification

The presence of large ripples on the Namib Dune's depositional slopes (Figures 11–13) highlights the possibility of large-ripple cross stratification appearing within sedimentary deposits on Mars, which, with the exception of granule-ripple stratification, has not been identified on Earth [*Lapotre et al.*, 2016]. How would large-ripple stratification manifest in the stratigraphic record? What is the significance of large-ripple stratification?

Although large ripples are not present on Earth, the style of stratification arising from the interaction of the large ripples and the lee slope could be similar to reworking of dune lee slopes by superimposed small dunes or wind ripples on Earth. Reworking of a slip face by ripples may be moderate, in which a short-lived, small change in the incidence angle generates impact ripples that overprint the grainflow surface (Figures 12, 16a, and 16b) or severe in which a long-lived, large change in incidence angle generates impact ripples that bevel the surface well below the angle of repose. In the former case, ripple stratification may be thin and intercalated with grainflow stratification (Figure 16c), while in the latter scenario, an erosional surface (i.e., reactivation surface) with a distinctly lower slope than the grainflow strata would form along with wind ripple stratification (Figure 16d). Reworking of the slip face during a change in wind is potentially more severe on Mars than on Earth because the strong feedback between the large-ripple topography and wind generates greater potential scour into the underlying sediment than is expected of typical terrestrial impact ripples.

Where ripple migration across the lee slope is coincident with deposition rather than erosion, large-ripple planar or trough cross stratification would form and become part of the primary dune stratification. Large-ripple stratification would appear similar to compound dune stratification on Earth (Figure 17a) [*Lapotre et al.*, 2016]. This type of stratification would be particularly expected on the most oblique portions of a dune slip face, such as the secondary slip face on Namib Dune where large ripples are migrating obliquely down the slope
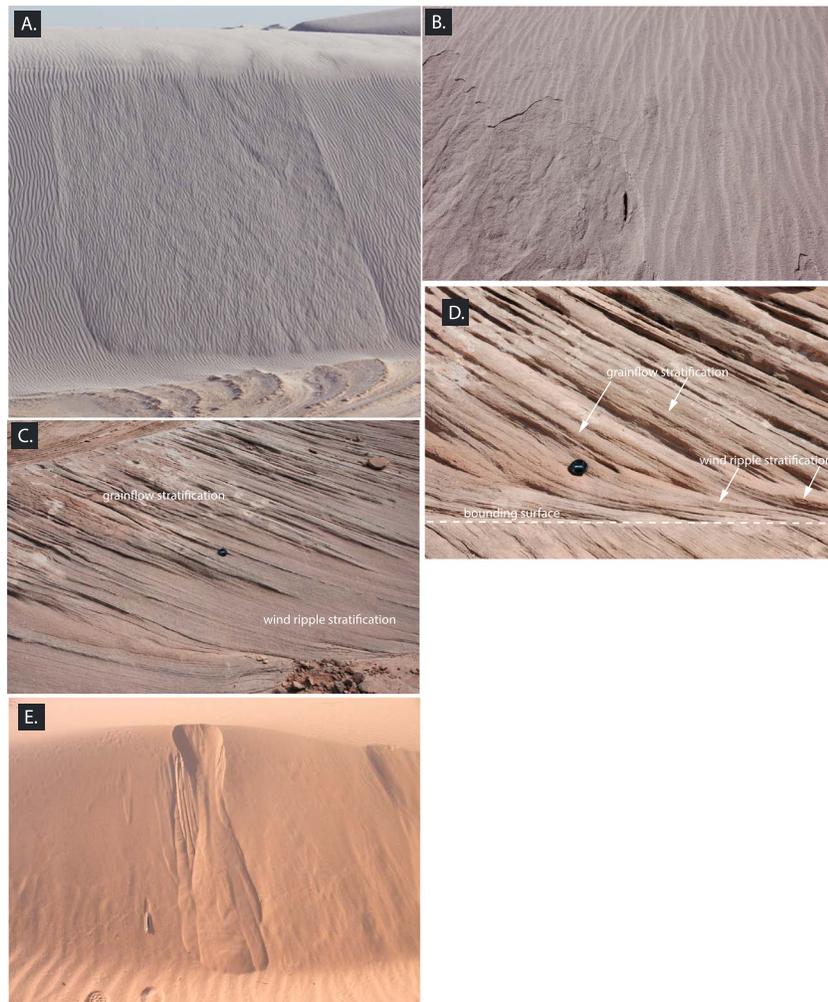
Figure 16. Modern and ancient eolian dune sedimentary structures on Earth. (a) Impact ripples overprinting grainflows at White Sands Dune Field, New Mexico, USA. (b) Impact ripples overprinting grainflows where the ripples have fractured because of the underlying grainflow relaxed to a lower angle at White Sands Dune Field, New Mexico, USA. (c and d) Eolian cross stratification in the Cedar Mesa Sandstone in southern Utah, USA. Grainflow stratification intercalated with wind ripple stratification. The grainflows stand out of the outcrop as "dagger-like" wedges (Figure 16c). The wind ripple stratification has a finer texture and makes up the majority of the base of the image. Grainflow stratification downlapping onto wind ripple stratification at the base of a set of stratification in the Cedar Mesa Sandstone, southern Utah, USA (Figure 16d). Note that the wind ripple stratification, which occupies the lower few centimeters of the image, makes up a small portion of the dune set in this location. (e) A typical grainflow on a sand dune at the Gran Desierto, Mexico. Note the hourglass shape with the scarp at the dune crest and the lobate toe. Note also the along-slope migrating impact ripples that make up the basal apron of the dune.

(Figure 13) or along the flanks of a linear, longitudinal dune (Figures 15a and 17b). Compound bed form stratification at Victoria crater in Meridiani Planum, Mars, was interpreted to result from the superposition of large ripples by *Lapotre et al.* [2016]. The development of planar versus trough compound cross stratification may depend on the degree to which the two- versus three-dimensionality of the large-ripple crest lines are affected by the lee slope angle [e.g., *Rubin*, 2012]. Planar stratification generated by two-dimensional crest lines might be expected where large ripples are forming on steeper lee slopes, whereas three-dimensional crest lines and trough cross stratification may be expected where ripples are forming on the lower slopes that might make up a sand sheet, secondary slip face, or the flanks of a linear dune.

Compound stratification may arise where large ripples migrate along the base of the lee slope, such as at Namib Dune (Figure 12). Although the basal apron at Namib Dune is small, where the basal apron is larger, large ripples may play a significant role in the basal lee slope processes and comprise a large component
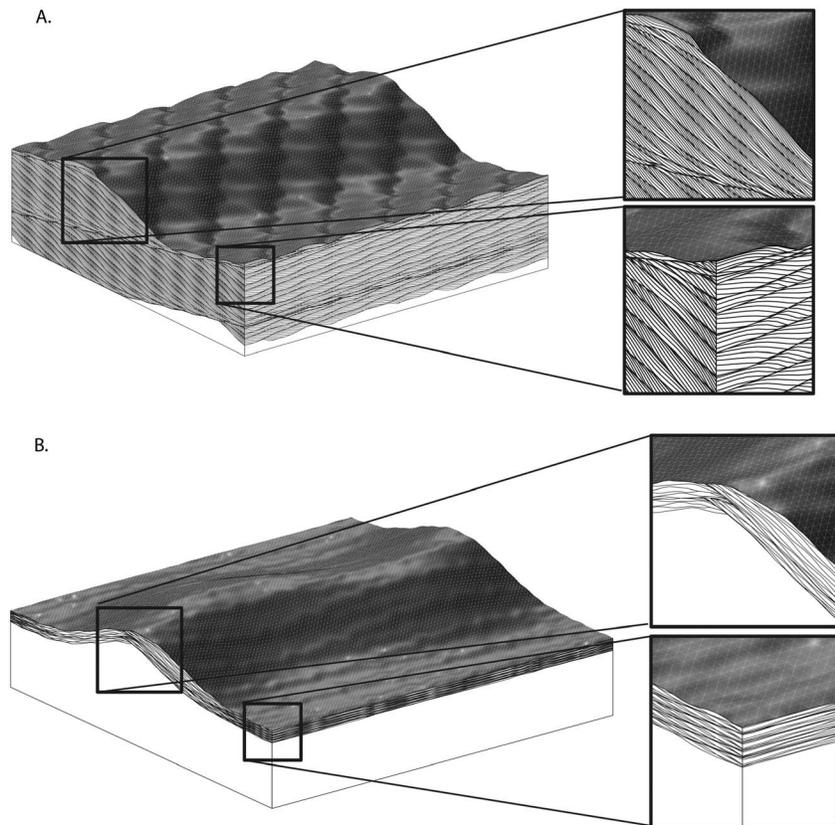
Figure 17. Models of cross stratification generated by compound bed forms. (a) Superimposed bed forms migrating obliquely down the depositional slope of a larger bed form generate stratification that is expected along the secondary lee slope of Namib Dune. This style of stratification was identified by *Lapotre et al.* [2016] in ancient eolian strata at Meridiani Planum, Mars. (b) Superimposed linear, longitudinal bed forms migrating along a linear bed form. This style of stratification would be expected in the linear dune area of the Bagnold Dune Field. Note that the absence of high-angle slopes in the linear bed form regime would limit the types of stratification present in the strata to those that form at less than the angle of repose (e.g., large and impact ripples).

of the cross stratification. Unlike ripples formed in the middle of the lee slope, ripples formed at the base of the dune have a higher probability of accumulation and preservation than those elsewhere on the primary lee slope because typically less than 10% of the slip face is preserved in the rock record [see *Lapotre et al.*, 2016]. For example, on oblique areas of a dune, bottom sets of cross stratification may be dominated by large-ripple stratification. As with the example of grainflows interfingering with impact ripples at Gobabeb large ripples (Figure 7), at the dune scale, grainflows may be buried by and interfinger with large-ripple stratification. As with the example given in Figures 17a and 17b, the stratification formed by ripples migrating along the basal plinth of the primary slip face of a dune would be similar to that forming on a compound crescentic or linear dune on Earth in which dunes move across the lee slope or basal plinth.

Recognizing large-ripple stratification is important because large-ripple size is thought to scale with atmospheric density such that lower atmospheric density generates larger ripples [*Lapotre et al.*, 2016]. Thus, the presence of large-ripple cross stratification implies a thin atmosphere at the time of formation [*Lapotre et al.*, 2016]. This rationale allowed *Lapotre et al.* [2016] to reinterpret cross stratification at Victoria crater in Meridiani Planum as large-ripple cross stratification based on the aforementioned criteria and suggests that Mars' atmosphere was thin at the time of deposition during the Late Noachian–Early Hesperian.

6.2. Grainflow, Grainfall, and Wind Ripple Stratification

Unlike the large ripples, which are not found on Earth, grainflow, grainfall, and impact ripples fall within the typical suite of eolian sedimentary structures found on Earth and the expectation is that these form Earth-like stratification. The grainflows found on Namib Dune and the large-ripple lee slopes have a typical sandflow,

hourglass shape with a lobate toe that extend partially or fully to the base of the dune or ripple (Figures 7 and 12). On Earth, grainflows are similarly shaped (Figure 16e) and grainflow stratification manifests as tabular inversely graded 2–5 cm stratification with a sharp, planar base (Figure 16d) [*Hunter*, 1977]. The grainflow toes are typically preserved as tongue-like laminae that taper to a point (Figure 16f), and because of the sorting processes during the flow of sand, the toe of the laminae is made of the coarsest fraction of the sand population. The same shape and distribution of grains (e.g., coarse grains at the toe – Figure 7a) are expected on Mars. If the size of the grainflows on Martian dunes is indeed larger as measured here (Table 1), the expectation would be somewhat thicker grainflow as part of the dune stratification. The grainflows formed on large ripples are much smaller than typical terrestrial grainflows and thus would form thinner grainflow stratification. Thin grainflow strata developed from large-ripple migration may be difficult to distinguish from grainfall or wind ripple stratification. Currently, no grainflow stratification has been identified in the Martian rock record.

Grainfall was only identified in the lee of large ripples. It appeared as a smooth featureless sand surface. The expected grainfall stratification is similar to that found on Earth with tabular 1–10 cm sharp or gradational based laminae that drape preexisting topography [*Hunter*, 1977], but as with the large-ripple grainflows, grainfall stratification formed on large ripples would likely be thinner. Impact ripples were ubiquitous across the primary lee slope of Namib Dune and around all areas of the large ripples. The size and shape of impact ripples on Mars are similar to those on Earth [*Lapotre et al.*, 2016], and the expected impact mechanism is thought to largely be the same [*Kok et al.*, 2012; *Durán et al.*, 2014]. Thus, wind ripple stratification formed on Mars should also be similar with the development of thin, planar, millimeter-scale, laminae with sharp, erosional bases and inverse grading [*Hunter*, 1977]. At Gobabeb, the wheel scuff revealed impact ripple stratification with the expected millimeter-scale lamination (Figure 7c) consistent with interpretations of impact ripple strata in Meridiani Planum and Gale crater [*Grotzinger et al.*, 2005, 2015; *Banham et al.*, 2016].

6.3. Field-Scale Distribution of Sedimentary Structures and Eolian Stratification Types

Curiosity's traverse through the Bagnold Dune Field, along with orbital image analysis, shows that sedimentary processes on the lee slopes vary in response to dune-modified secondary flows, primary wind flows, and spatial position within the dune field. Combined, these components suggest that the overall distribution of sedimentary processes within the dune field can be considered a function of the dune-field pattern, which reflects a history of self-organization through dune-dune interactions and climate and basin topography-influenced wind events [*Kocurek and Ewing*, 2005, 2016b].

As with other crater-basin dune fields, the pattern at Bagnold Dune Field emerges within complex boundary conditions and is characterized by dune types that vary as a function of sediment supply and wind regime [*Fenton et al.*, 2003; *Hayward et al.*, 2007; *Silvestro et al.*, 2013]. In turn, the distribution of sedimentary processes varies with different dune types. Angle-of-repose slopes primarily occur within the barchan dunes proximal to the northern margin of the dune field, whereas lower-angled slopes occur within sand sheets and linear dunes at the center and southeastern margin of the dune field proximal to Mount Sharp. Cast in terms of the distribution of sedimentary processes and potential stratification types, processes associated with angle-of-repose slopes such as grainflow and grainfall will be more prominent in the northern Bagnold Dune Field margin, whereas large ripple and impact ripples dominate the core of the dune field. Thus, the potential distribution of stratification types generated by the Bagnold Dune Field in its current state is one in which large-ripple and impact ripple stratification would make up most of the body of strata, and dune grainflow and grainfall stratification would make up a relatively small overall fraction of stratification. Impact ripple stratification would dominate the stratification where linear, longitudinal large ripples are migrating across linear dunes and sand sheets because, as shown by the example of large ripples at the convergence of the Namib Dune slip faces, there is an absence of angle of repose slopes on these ripples and impact ripples migrate along the crests of longitudinally extending ripples.

The geomorphic distribution of sedimentary processes, however, is not an accurate representation of the distribution of sedimentary structures within the potential stratification. The accumulation of strata could not occur across much of the dune field because of the difference between sediment availability versus transport-limited conditions. The barchan area, for example, is sediment availability limited and the potential for accumulation in this area is limited to topographic lows, such as small craters, across which the dunes migrate. In contrast, the sand sheet and linear dune areas of the core of the field are transport limited in a

zone of wind convergence as implied by the dune morphology and thus have greater potential accumulation. The distribution of stratification types is thus not only a function of the distribution of depositional slopes determined by the dune-field pattern but of the distribution of depositional slopes within areas with the potential for accumulation.

7. Conclusions

Curiosity's traverse through the Bagnold Dune Field highlighted both uniquely Martian and terrestrial-like sedimentary processes. One of the most striking discoveries of the campaign was the observation that two scales of ripples are superimposed on the dunes [*Lapotre et al.*, 2016]. This observation cannot be easily explained by current models of wind impact ripples or differences in grain size and thus requires new models of wind-blown bed forms to be explored [*Lapotre et al.*, 2016]. The formation of large ripples as a uniquely Martian process stands in contrast to observations of many terrestrial-like sedimentary processes occurring on the ripples and dunes. Slope analysis of HiRISE DEMs show that the topography of the dunes encountered by Curiosity is similar to that of terrestrial barchan dunes. The angles of the stoss slopes of the dunes fall within a typical range found on Earth (e.g., ~7°–10°). The lee slope of the dunes, as measured from HiRISE and Mastcam-generated DEMs, average about 29°, which is typical of the angle of repose on Earth. These slope measurements are consistent with the presence of grainflows across the lee face. The grainflow scarps and lobes measure somewhat larger than reported for terrestrial analogs but do not appear outside of the typical grainflow range. While the grainflows on the large ripples are smaller in size than those on the dune, they occur at the same 29° angle and have approximately the same scarp and lobe size ratios as dune-scale grainflows. Grainfall, though not found on the dune slip face, is present on the large ripples and, where adjacent to grainflows, forms at angles up to 40° with more common measurements around 32°–33°, which is inferred to be close to the static angle of repose for these grains.

The presence of an additional scale of ripple on the dunes provides a novel means by which winds can be interpreted from bed form morphology. Because the impact ripples, large ripples, and dunes are different in size, they also respond to, and potentially reflect, different components and timescales of winds at Gale crater [*Rubin and Ikeda*, 1990; *Werner and Kocurek*, 1997; *Ewing et al.*, 2015]. The large ripples formed in the interdune area around Namib Dune that appear to be longitudinally extending away from the horn of Namib Dune imply the convergence of two winds, which is consistent with bimodal winds as inferred from the dune morphology [*Hobbs et al.*, 2010; *Silvestro et al.*, 2013; *Day and Kocurek*, 2015]. Large-ripple morphology at the base of Namib Dune's lee slope indicates that one wind is from the southeast, and the large-ripple morphology at the base of the stoss slope of High Dune indicates one wind from the west. The presence of two winds is supported by recent REMS data and can be explained by diurnal cycling of upslope and downslope winds [*Newman et al.*, 2017]. The presence of large ripples at Gobabeb that are oriented in the same direction as surrounding impact ripples and differently from surrounding large ripples implies that the large ripples at Gobabeb do not reflect the overall, seasonal wind regime but rather reflect the wind regime that created the impact ripples. Given the maximum measured migration rates within the dune field [*Silvestro et al.*, 2016], the orientation of these ripples could represent a response to a month long wind regime within the overall seasonal cycle.

Based upon observations of modern sedimentary processes at the Bagnold Dune Field, the null hypothesis that the Martian rock record is the same as that found on Earth is rejected. However, the extent of the difference between Earth and Mars mainly relates to the potential presence of large-ripple stratification in Martian eolian stratification. Other aspects of the stratigraphy are likely similar to the terrestrial rock record. As shown by *Lapotre et al.* [2016], large ripples have likely played a role in the development of the Martian eolian rock record, but similarities in modern grainflow, grainfall, and impact ripples point to the part of the Martian stratigraphic record that should be similar to that on Earth. Large-ripple stratification may be unique, but detecting the presence of this stratification could be hindered by recognizing distinctive textures in the small (decimeter)-scale stratification and by the potentially limited presence of large-ripple stratification within accumulated stratigraphy. The presence of large-ripple stratification in the rock record depends on the distribution of oblique and longitudinal depositional slopes determined by the dune-field pattern, which is in turn influenced by the wind regime of the basin. With those conditions satisfied, the large ripples must also occur in an area of the basin in which eolian stratification is accumulating rather than in bypass.

Thus, while the presence of large ripples dictates that the Martian rock record must be different from the terrestrial record, like Earth, the basin-scale boundary conditions controlling dune-field pattern development will strongly determine the distribution of stratification types and the architecture of the Martian eolian rock record.

References

Achilles, C. N., et al. (2017), Mineralogy of active eolian sediment from the Namib Dune, Gale crater, Mars, *J. Geophys. Res. Planets*, *122*, doi:10.1002/2017JE005262.

Allen, J. R. L. (1970), The avalanching of granular solids on dune and similar slopes, *J. Geol.*, *78*, 326–351.

Anderson, R. B., and J. F. Bell III (2010), Geologic mapping and characterization of Gale crater and implications for its potential as a Mars Science Laboratory landing site, *Mars*, *5*, 76–128.

Atwood-Stone, C., and A. S. McEwen (2013), Avalanche slope angles in low-gravity environments from active Martian sand dunes, *Geophys. Res. Lett.*, *40*, 2929–2934, doi:10.1002/grl.50586.

Bagnold, R. A. (1941), *The Physics of Wind Blown Sand and Desert Dunes*, vol. 265(10), 244 pp., Methuen & Co., London.

Baitis, E., G. Kocurek, V. Smith, D. Mohrig, R. C. Ewing, and A. P. Peyret (2014), Definition and origin of the dune-field pattern at White Sands, New Mexico, *Aeolian Res.*, *15*, 269–287.

Balme, M., D. C. Berman, M. C. Bourke, and J. R. Zimbelman (2008), Transverse aeolian ridges (TARs) on Mars, *Geomorphology*, *101*(4), 703–720.

Banham, S. G., S. Gupta, D. M. Rubin, J. A. Watkins, D. Y. Sumner, J. P. Grotzinger, K. W. Lewis, K. S. Edgett, L. A. Edgar, and K. M. Stack (2016), Reconstruction of an ancient eolian Dune Field at Gale crater, Mars: Sedimentary analysis of the Stimson formation, Lunar and Planet. Sci. Conf., vol. 47, p. 2346.

Bennett, S. J., and J. L. Best (1995), Mean flow and turbulence structure over fixed, two-dimensional dunes: Implications for sediment transport and bedform stability, *Sedimentology*, *42*(3), 491–513.

Bourke, M. C., and H. A. Viles (2016), Valley floor aeolianite in an equatorial pit crater on Mars, *Geophys. Res. Lett.*, *43*, 12,356–12,362, doi:10.1002/2016GL071467.

Breed, C. S., and T. Grow (1979), Morphology and distribution of dunes in sand seas observed by remote sensing, in *A Study of Global Sand Seas*, vol. 1052, pp. 253–302, U.S. Gov. Print. Office, Washington, D. C.

Bridges, N. T., P. E. Geissler, A. S. McEwen, B. J. Thomson, F. C. Chuang, K. E. Herkenhoff, L. P. Keszthelyi, and S. Martínez-Alonso (2007), Windy Mars: A dynamic planet as seen by the HiRISE camera, *Geophys. Res. Lett.*, *34*, L23205, doi:10.1029/2007GL031445.

Bridges, N. T., et al. (2012), Planet-wide sand motion on Mars, *Geology*, *40*(1), 31–34.

Bridges, N. T., et al. (2017), Martian aeolian activity at the Bagnold Dunes, Gale crater: The view from the surface and orbit, *J. Geophys. Res. Planets*, *122*, doi:10.1002/2017JE005263.

Brookfield, M. E. (1977), The origin of bounding surfaces in ancient aeolian sandstones, *Sedimentology*, *24*(3), 303–332.

Brothers, S. (2016), Aeolian dune dynamics and the stratigraphic record, Dissertation, Univ. Texas at Austin.

Bunte, K., and S. R. Abt (2001), Sampling surface and subsurface particle-size distributions in wadable gravel-and cobble-bed streams for analyses in sediment transport, hydraulics, and streambed monitoring, *Gen. Tech. Rep. RMRS-GTR-74*, 428 pp., Dep. of Agric., For. Serv., Rocky Mt. Res. Stn., Fort Collins, Colo.

Cardinale, M., S. Silvestro, D. A. Vaz, T. Michaels, M. C. Bourke, G. Komatsu, and L. Marinangeli (2016), Present-day aeolian activity in Herschel crater, Mars, *Icarus*, *265*, 139–148.

Carrigy, M. A. (1970), Experiments on the angles of repose of granular materials 1, *Sedimentology*, *14*(3–4), 147–158.

Chojnacki, M., D. M. Burr, J. E. Moersch, and T. I. Michaels (2011), Orbital observations of contemporary dune activity in Endeavor crater, Meridiani Planum, Mars, *J. Geophys. Res.*, *116*, E00F19, doi:10.1029/2010JE003675.

Claudin, P., and B. Andreotti (2006), A scaling law for aeolian dunes on Mars, Venus, Earth, and for subaqueous ripples, *Earth Planet. Sci. Lett.*, *252*(1), 30–44.

Cousin, A., et al. (2017), Geochemistry of the Bagnold Dune Field as observed by ChemCam and comparison with other aeolian deposits at Gale Crater, *J. Geophys. Res. Planets*, *122*, doi:10.1002/2017JE005261.

Cutts, J. A., and R. S. U. Smith (1973), Eolian deposits and dunes on Mars, *J. Geophys. Res.*, *78*, 4139–4154, doi:10.1029/JB078i020p04139.

Dalrymple, R. W., and R. N. Rhodes (1995), Estuarine dunes and bars, *Dev. Sedimentol.*, *53*, 359–422.

Day, M., and G. Kocurek (2015), Observations of an aeolian landscape: From surface to orbit in gale crater, *Icarus*, *280*, 37–71.

du Pont, S. C., C. Narteau, and X. Gao (2014), Two modes for dune orientation, *Geology*, *42*(9), 743–746.

Durán, O., P. Claudin, and B. Andreotti (2014), Direct numerical simulations of aeolian sand ripples, *Proc. Natl. Acad. Sci. U.S.A.*, *111*(44), 15,665–15,668.

Eastwood, E. N., G. Kocurek, D. Mohrig, and T. Swanson (2012), Methodology for reconstructing wind direction, wind speed and duration of wind events from aeolian cross-strata, *J. Geophys. Res.*, *117*, F03035, doi:10.1029/2012JF002368.

Edgett, K. S., et al. (2012), Curiosity's Mars hand lens imager (MAHLI) investigation, *Space Sci. Rev.*, *170*(1–4), 259–317.

Edwards, C. S., S. Piqueux, V. E. Hamilton, R. L. Fergason, K. E. Herkenhoff, A. R. Vasavada, L. Sacks, K. Lewis, and M. D. Smith (2017), The thermophysical properties of the Bagnold Dunes, Mars: Ground-truthing orbital data, http://arxiv.org/abs/1711.10699.

Elhmann, B. L., et al. (2017), Chemistry, mineralogy, and grain size of the Bagnold Dune Field: A synthesis of MSL Curiosity observations revealing size-sorting, mafic enrichment and volatile depletion, *J. Geophys. Res. Planets*, *122*, doi:10.1002/2017JE005267.

Ewing, R. C., and G. A. Kocurek (2010), Aeolian dune interactions and dune-field pattern formation: White Sands Dune Field, New Mexico, *Sedimentology*, *57*(5), 1199–1219.

Ewing, R. C., A. P. B. Peyret, G. Kocurek, and M. Bourke (2010), Dune field pattern formation and recent transporting winds in the Olympia Undae Dune Field, north polar region of Mars, *J. Geophys. Res.*, *115*, E08005, doi:10.1029/2009JE003526.

Ewing, R. C., G. D. McDonald, and A. G. Hayes (2015), Multi-spatial analysis of aeolian dune-field patterns. *Geomorphology*, *240*, 44–53.

Fenton, L. K., J. L. Bandfield, and A. Ward (2003), Aeolian processes in Proctor crater on Mars: Sedimentary history as analyzed from multiple data sets, *J. Geophys. Res.*, *108*(E12), 5129, doi:10.1029/2002JE002015.

Finkel, H. J. (1959), The barchans of southern Peru, *J. Geol.*, *67*(6), 614–647.

Gao, X., C. Narteau, and O. Rozier (2015), Development and steady states of transverse dunes: A numerical analysis of dune pattern coarsening and giant dunes, *J. Geophys. Res. Earth*, *120*, 2200–2219, doi:10.1002/2015JF003549.

Gómez-Elvira, J., et al. (2012), REMS: The environmental sensor suite for the Mars Science Laboratory rover, *Space Sci. Rev.*, *170*(1–4), 583–640.

Greeley, R., et al. (1992), Aeolian features on Venus: Preliminary Magellan results, *J. Geophys. Res.*, *97*, 13,319–13,345, doi:10.1029/92JE00980.

Greeley, R., and J. D. Iversen (1985), Wind as a Geological Process, 333 pp., Cambridge Univ. Process, New York.

Greeley, R., R. Leach, B. White, J. Iversen, and J. Pollack (1980), Threshold windspeeds for sand on Mars: Wind tunnel simulations, *Geophys. Res. Lett.*, *7*, 121–124, doi:10.1029/GL007i002p00121.

Grotzinger, J. P., et al. (2005), Stratigraphy and sedimentology of a dry to wet eolian depositional system, Burns formation, Meridiani Planum, Mars, *Earth Planet. Sci. Lett.*, *240*(1), 11–72.

Grotzinger, J. P., et al. (2015), Deposition, exhumation, and paleoclimate of an ancient lake deposit, deposition, exhumation, and paleoclimate of an ancient lake deposit, Gale crater, Mars, *Science*, *350*(6257), aac7575.

Hayward, R. K., K. F. Mullins, L. K. Fenton, T. M. Hare, T. N. Titus, M. C. Bourke, A. Colaprete, and P. R. Christensen (2007), Mars Global Digital Dune Database and initial science results, *J. Geophys. Res.*, *112*, E11007, doi:10.1029/2007JE002943.

Herkenhoff, K. E., S. Byrne, P. S. Russell, K. E. Fishbaugh, and A. S. McEwen (2007), Meter-scale morphology of the north polar region of Mars, *Science*, *317*(5845), 1711–1715.

Hesp, P. A., and K. Hastings (1998), Width, height and slope relationships and aerodynamic maintenance of barchans, *Geomorphology*, *22*(2), 193–204.

Hobbs, S. W., D. J. Paull, and M. C. Bourke (2010), Aeolian processes and dune morphology in Gale crater, *Icarus*, *210*(1), 102–115.

Hunter, R. E. (1977), Basic types of stratification in small eolian dunes, *Sedimentology*, *24*(3), 361–387.

Jackson, D. W., M. C. Bourke, and T. A. Smyth (2015), The dune effect on sand-transporting winds on Mars. *Nat. Commun.*, *6*, doi:10.1038/ncomms9796.

Jia, P., B. Andreotti, and P. Claudin (2017), Giant ripples on comet 67P/Churyumov–Gerasimenko sculpted by sunset thermal wind, *Proc. Natl. Acad. Sci.*, *114*(10), 2509–2514.

Johnson, J. R., et al. (2017), Visible/near-infrared spectral diversity from in situ observations of the Bagnold Dune Field sands in Gale crater, Mars, *J. Geophys. Res. Planets*, *122*, doi:10.1002/2016JE005187.

Kleinhans, M. G. (2004), Sorting in grain flows at the lee side of dunes, *Earth Sci. Rev.*, *65*(1), 75–102.

Kleinhans, M. G., H. Markies, S. J. de Vet, and F. N. Postema (2011), Static and dynamic angles of repose in loose granular materials under reduced gravity, *J. Geophys. Res.*, *116*, E11004, doi:10.1029/2011JE003865.

Kocurek, G., and R. C. Ewing (2005), Aeolian dune field self-organization—Implications for the formation of simple versus complex dune-field patterns, *Geomorphology*, *72*(1), 94–105.

Kocurek, G., and R. C. Ewing (2016a), Source-to-sink; an Earth/Mars comparison of boundary conditions for eolian dune systems, in *Sedimentary Geology of Mars*, *Spec. Publ.*, vol. 102, edited by J. P. Grotzinger and R. E. Milliken, pp. 151–168, SEPM (Society for Sedimentary Geology), Tulsa, Okla.

Kocurek, G., and R. C. Ewing, (2016b), Trickle-Down and Trickle-Up Boundary Conditions in Eolian Dune-Field Pattern Formation, in *Autogenic Dynamics and Self-Organization in Sedimentary Systems*, *Spec. Publ.*, vol. 106, edited by D. A. Budd, E. A. Hajek, and S. J Purkis, pp. 5–17, SEPM (Society for Sedimentary Geology), Tulsa, Okla., doi:10.2110/sepmsp.106.04.

Kok, J. F. (2010), An improved parameterization of wind-blown sand flux on Mars that includes the effect of hysteresis, *Geophys. Res. Lett.*, *37*, L12202, doi:10.1029/2010GL043646.

Kok, J. F., E. J. Parteli, T. I. Michaels, and D. B. Karam (2012), The physics of wind-blown sand and dust, *Rep. Prog. Phys.*, *75*(10), 106901.

Lapotre, M. G. A., et al. (2016), Large wind ripples on Mars: A record of atmospheric evolution, *Science*, *353*(6294), 55–58.

Lapotre, M. G. A., M. P. Lamb, and B. McElroy (2017), What sets the size of current ripples?, *Geology*, *45*, 243–246.

Lorenz, R. D., et al. (2006), The sand seas of Titan: Cassini RADAR observations of longitudinal dunes, *Science*, *312*(5774), 724–727.

Lowe, D. R. (1976), Grain flow and grain flow deposits, *J. Sediment. Res.*, *46*(1), 188–199.

Maurice, S., et al. (2012), The ChemCam instrument suite on the Mars Science Laboratory (MSL) rover: Science objectives and mast unit description, *Space Sci. Rev.*, *170*(1–4), 95–166.

McEwen, A. S., et al. (2007), Mars reconnaissance orbiter's high resolution imaging science experiment (HiRISE), *J. Geophys. Res.*, *112*, E05S02, doi:10.1029/2005JE002605.

Malin, M. C., et al. (2010), The Mars Science Laboratory (MSL) mast-mounted cameras (Mastcams) flight instruments, in *Lunar and Planetary Science Conference*, vol. 41, 1123 pp.

Milliken, R. E., R. C. Ewing, W. W. Fischer, and J. Hurowitz (2014), Wind-blown sandstones cemented by sulfate and clay minerals in Gale crater, Mars, *Geophys. Res. Lett.*, *41*, 1149–1154, doi:10.1002/2013GL059097.

Moore, J. M., et al. (2017), Sublimation as a landform-shaping process on Pluto, *Icarus*, *287*, 320–333

Mottola, S., et al. (2015), The structure of the regolith on 67P/Churyumov-Gerasimenko from ROLIS descent imaging, *Science*, *349*(6247), aab0232.

Newman, C., et al. (2017), Winds measured by the Rover Environmental Monitoring Station (REMS) during the Mars Science Laboratory (MSL) rover's Bagnold Dunes campaign and comparison with numerical modeling using MarsWRF, *Icarus*, *291*, 203–231.

Nield, J. M., G. F. Wiggs, M. C. Baddock, and M. H. Hipondoka (2017), Coupling leeside grainfall to avalanche characteristics in aeolian dune dynamics, *Geology*, *45*(3), 271–274.

O'Connell-Cooper, C. D., J. G. Spray, L. M. Thompson, R. Gellert, J. A. Berger, N. I. Boyd, E. D. Desouza, G. M. Perrett, M. Schmidt, and S. J. VanBommel (2017), APXS-derived chemistry of the Bagnold dune sands: Comparisons with Gale Crater soils and the global Martian average, *J. Geophys. Res. Planets*, *122*, doi:10.1002/2017JE005268.

Pähtz, T., Kok, J. F., Parteli, E.J. and Herrmann, H. J. (2013), Flux saturation length of sediment transport, *Phys. Rev. Lett.*, *111*(21), 218002.

Parteli, E. J., Durán, O., Bourke, M. C., Tsoar, H., Pöschel, T., and Herrmann, H. (2014), Origins of barchan dune asymmetry: Insights from numerical simulations. *Aeolian Res.*, *12*, 121–133.

Pelletier, J. D., D. J. Sherman, J. T. Ellis, E. J. Farrell, N. L. Jackson, B. Li, K. F. Nordstrom, L. P. Maia, and M. Omidyeganeh (2015), Dynamics of sediment storage and release on aeolian dune slip faces: A field study in Jericoacoara, Brazil, *J. Geophys. Res. Earth Surf.*, *120*, 1911–1934, doi:10.1002/2015JF003636.

Reffet, E., S. C. du Pont, P. Hersen, and S. Douady (2010), Formation and stability of transverse and longitudinal sand dunes, *Geology*, *38*(6), 491–494.

Rubin, D. M. (2012), A unifying model for planform straightness of ripples and dunes in air and water, *Earth Sci. Rev.*, *113*(3), 176–185.

Rubin, D. M., and R. E. Hunter (1985), Why deposits of longitudinal dunes are rarely recognized in the geologic record, *Sedimentology*, *32*(1), 147–157.

Rubin, D. M., and R. E. Hunter (1987), Bedform alignment in directionally varying flows, *Science*, *237*(4812), 276–278.

Rubin, D. M., and H. Ikeda (1990), Flume experiments on the alignment of transverse, oblique, and longitudinal dunes in directionally varying flows, *Sedimentology*, *37*(4), 673–684.

Rubin, D. M., and P. A. Hesp (2009), Multiple origins of linear dunes on Earth and Titan, *Nat. Geosci.*, 2(9), 653–658.

Schatz, V., H. Tsoar, K. S. Edgett, E. J. R. Parteli, and H. J. Herrmann (2006), Evidence for indurated sand dunes in the Martian north polar region, *J. Geophys. Res.*, 111, E04006, doi:10.1029/2005JE002514.

Schmidt, F., F. Andrieu, F. Costard, M. Kocifaj, and A. G. Meresescu (2017), Formation of recurring slope lineae on Mars by rarefied gas-triggered granular flows, *Nat. Geosci.*, 10, 270–273.

Seelos, K. D., F. P. Seelos, C. E. Viviano-Beck, S. L. Murchie, R. E. Arvidson, B. L. Ehlmann, and A. A. Fraeman (2014), Mineralogy of the MSL *Curiosity* landing site in Gale crater as observed by MRO/CRISM, *Geophys. Res. Lett.*, 41, 4880–4887, doi:10.1002/2014GL060310.

Sharp, R. P. (1963), Wind ripples, *J. Geol.*, 71, 617–636.

Silvestro, S., D. A. Vaz, R. C. Ewing, A. P. Rossi, L. K. Fenton, T. I. Michaels, J. Flahaut, and P. E. Geissler (2013), Pervasive aeolian activity along rover Curiosity's traverse in Gale crater, Mars, *Geology*, 41(4), 483–486.

Silvestro, S., D. A. Vaz, H. Yizhaq, and F. Esposito (2016), Dune-like dynamic of Martian aeolian large ripples, *Geophys. Res. Lett.*, 43, 8384–8389, doi:10.1002/2016GL070014.

Southard, J. B., and L. A. Boguchwal (1990), Bed configurations in steady unidirectional water flows. Part 2. Synthesis of flume data, *J. Sediment. Res.*, 60(5).

Sullivan, R., et al. (2008), Wind-driven particle mobility on Mars: Insights from Mars Exploration Rover observations at "El Dorado" and surroundings at Gusev crater, *J. Geophys. Res.*, 113, E06S07, doi:10.1029/2008JE003101.

Sullivan, R., and J. Kok (2017), Aeolian saltation on Mars at low to moderate wind speeds, *J. Geophys. Res. Planets*, 122, doi:10.1002/2017JE005275.

Sutton, S. L. F., C. McKenna Neuman, and W. Nickling (2013), Avalanche grainflow on a simulated aeolian dune, *J. Geophys. Res. Earth*, 118, 1767–1776, doi:10.1002/jgrf.20130.

Swanson, T., D. Mohrig, and G. Kocurek (2016), Aeolian dune sediment flux variability over an annual cycle of wind, *Sedimentology*, 63(6), 1753–1764.

Sweet, M. L., and G. Kocurek (1990), An empirical model of aeolian dune lee-face airflow, *Sedimentology*, 37(6), 1023–1038.

Thomson, B. J., N. T. Bridges, and R. Greeley (2008), Rock abrasion features in the Columbia Hills, Mars, *J. Geophys. Res.*, 113, E08010, doi:10.1029/2007JE003018.

Tsoar, H., R. Greeley, and A. R. Peterfreund (1979), Mars: The north polar sand sea and related wind patterns, *J. Geophys. Res.*, 84, 8167–8180, doi:10.1029/JB084iB14p08167.

Tsoar, H. (1983), Dynamic processes acting on a longitudinal (seif) sand dune, *Sedimentology*, 30(4), 567–578.

Vaz, D. A., S. Silvestro, P. T. Sarmento, and M. Cardinale (2016), Migrating meter-scale bedforms on Martian dark dunes: Are terrestrial aeolian ripples good analogues?, *Aeolian Res.*, 26, 101–116.

Walker, I. J., and W. G. Nickling (2002), Dynamics of secondary airflow and sediment transport over and in the lee of transverse dunes, *Prog. Phys. Geogr.*, 26(1), 47–75.

Werner, B. T., and G. Kocurek (1997), Bed-form dynamics: Does the tail wag the dog?, *Geology*, 25(9), 771–774.

Wiggs, G. F., I. Livingstone, and A. Warren (1996), The role of streamline curvature in sand dune dynamics: Evidence from field and wind tunnel measurements, *Geomorphology*, 17(1), 29–46.

Yalin, M. S. (1985), On the determination of ripple geometry, *J. Hydraul. Eng.*, 111(8), 1148–1155.

Yizhaq, H., I. Katra, O. Isenberg, and H. Tsoar (2012), Evolution of megaripples from a flat bed, *Aeolian Res.*, 6, 1–12.